AN ABSTRACT OF THE THESIS OF

Gautam Jayant Sopal for the degree of Master of Science in Civil Engineering presented on December 15, 2008.

Title: Environmental Durability of Reinforced Concrete Deck Girders Strengthened with Surface-Bonded Carbon Fiber-Reinforced Polymer.

Abstract approved:

Christopher C. Higgins

Long-term durability of surface-bonded carbon fiber-reinforced polymer (CFRP) for shear strengthening of reinforced concrete (RC) bridge members remains uncertain due to the limited field experience with these materials. This paper provides experimental results from the testing of full-scale RC bridge girder specimens after exposure to prolonged environmental exposure and combined action of freeze-thaw + repeated service loads. CFRP shear contributions seen in experimental results were estimated using a refined base capacity prediction (Response-2000) and compared to predicted CFRP shear contributions (ACI-440). The IT specimens did not exhibit strength reductions due to moisture exposure, instead the presence of continuous water exposure for the relatively young concrete caused higher concrete tensile properties resulting in increased bond strength.

Previous research showed CFRP strengthened T specimens with freeze-thaw exposure exhibited lower shear capacity than similar unexposed CFRP strengthened T specimen. But the current research demonstrated that if the beam is well protected against moisture infiltration at the strip termination, the beam will be less susceptible to freeze-thaw bond deterioration. The orientations of specimens during repair and during exposure are important considerations for environmental durability. The CFRP strip terminations should be focused on during installation to insure well and perhaps extra saturation even past the CFRP material to limit moisture infiltration along this edge.

Environmental Durability of Reinforced Concrete Deck Girders Strengthened with Surface-Bonded Carbon Fiber-Reinforced Polymer

by

Gautam Jayant Sopal

A THESIS

submitted to

Oregon State University

in partial fulfillment of

the requirements for the

degree of

Master of Science

Presented December 15, 2008

Commencement June, 2009

Master of Science thesis of Gautam Jayant Sopal

presented on December 15, 2008.

APPROVED:

Major Professor, representing Civil Engineering

Head of the School of Civil and Construction Engineering

Dean of the Graduate School

I understand that my thesis will become part of the permanent collection of Oregon State University libraries. My signature below authorizes release of my thesis to any reader upon request.

Gautam Jayant Sopal, Author

ACKNOWLEDGEMENTS

First, I would like to express my sincere appreciation to Dr. Christopher Higgins for his continuous support and invaluable guidance throughout my research and analysis. I thank him for entrusting me with a very interesting research project, and providing me this great opportunity to contribute to academia. The author also wishes to thank the following graduate students for their assistance with laboratory experimentation and in critically discussing the findings of this research: Ekin Senturk , Tugrul Turan, Duncan Stark, Josh Udall, Matt Dawson, Dan Howell, Mikal Mitchell, Thomas Schumacher.

This research was funded by the Oregon Transportation Research and Education Consortium (OTREC) and the Oregon Department of Transportation (ODOT) as part of a larger study on the environmental durability of carbon fiber-reinforced polymers (CFRP). CFRP materials were donated by the BASF Corporation.

Finally, I would like to thank to my parents, my relatives and my friends, for their unconditional support and understanding, I appreciate that you have always been there for me.

TABLE OF CONTENTS

TABLE OF CONTENTS (Continued)

Page

TABLE OF CONTENTS (Continued)

LIST OF FIGURES

LIST OF FIGURES (Continued)

LIST OF FIGURES (Continued)

LIST OF TABLES

ENVIRONMENTAL DURABILITY OF REINFORCED CONCRETE DECK GIRDERS STRENGTHENED WITH SURFACE-BONDED CARBON FIBER-REINFORCED POLYMER

INTRODUCTION

Many of mid-twentieth century reinforced concrete deck girder (RCDG) bridges in the State of Oregon are considered deficient for shear. These RCDG bridges, with relatively light shear reinforcement and poor flexural details, commonly exhibit diagonal cracks resulting from increased service load magnitudes and volumes. With the large population of cracked bridges and limited resources available for replacements, effective repair methods are needed. Repair of civil infrastructure has become a key market for composites and externally bonded fiber reinforced polymers (FRP) particularly have found many applications. FRP is typically comprised of high strength fibers (e.g., carbon, glass, aramid) saturated with a polyester or vinyl ester resin resulting in a composite material with mechanical properties better than either of the components. These materials are applied as additional shear stirrups and flexural reinforcement, which have been shown to enhance ductility, strength and stiffness of the member in the short term. The recent development of these materials for civil infrastructure means that there is no historical record of long-term durability and thus the performance and life of FRP strengthened members subjected to environmental exposure is uncertain.

BACKGROUND

Most of the transportation infrastructure in the US was constructed in the middle of the 20th century and is approaching the end of its expected design life. In addition, there were significant increases in load demands over that period. To extend the life of existing infrastructure there is a need for fast, efficient, and durable strengthening methods. A constantly growing need for new and improved materials, processes, and products for cost effective manufacture and design of engineering structures and systems has been driving force in the development of the composite materials for structural applications. One of the techniques gaining popularity is the bonding of CFRP sheets or laminates on structural elements such as reinforced concrete beams and columns. The high strength-to-weight ratios and conformability to the existing structure make CFRP attractive materials for infrastructure rehabilitation.

A significant amount of prior research has been done on the performance of reinforced concrete beams retrofitted for shear and flexure with CFRP composites (Chajes *et al*. 1995, Malvar *et al*. 1995, Sato 1996, Norris *et al*. 1997, Triantafillou 1998, Buyukozturk *et al.*1998, Shehata *et al*. 2000, Al-Mahaidi *et al*. 2001, Li *et al*. 2001, Chen and Teng 2003, Zhang *et al.*2005, Higgins *et al*.2006). However, a little work has examined the effects of environmental exposure on the behavior of strengthened members considering long-term performance.

Although applications of this type of strengthening for bridge members have been reported in the literature, many designers are still concerned by the long-term durability of these materials, especially when they are used under adverse environmental conditions such as freeze-thaw cycling, moisture ingress, fatigue loading and in particular, combinations of

that exposure. A recent survey of transportation agencies in 2005 indicated that field applications of CFRP for shear strengthening have been in–service less than 10 years [Higgins *et al.* 2006]. Due to the lack of field performance data, long-term durability of FRP materials is typically predicted using accelerated laboratory tests. CFRP strengthening can be used to provide additional flexural or shear strength and the performance depends on stress transfer between the concrete and CFRP laminate. Ideally designers desire a CFRP laminates that are perfectly bonded to the concrete substrate. Unfortunately, perfect bonding does not exist and bond failure can occur. The types, causes, and mechanisms of bond failure are complex and varied, and a considerable research has focused on characterization of bond stresses, bond development lengths, and failure of bond FRP reinforcement on concrete. A limited database of information exists on the effects of environmental conditions on performance of the bond between the CFRP reinforcement and substrate material. The effects of moisture and temperature cycling of the concrete on the bond strength between concrete and CFRP reinforcement is still not well understood or documented. American Concrete Institute (ACI) Committee 440.2R requires minimum bond strength of 200 psi (1.4 MPa) and a failure mode expected within the concrete substrate.

The key environmental exposures that may affect CFRP performance for most bridge applications include: temperature, moisture, fatigue, and combined effects. These are details subsequently.

Temperature

Based on review of the literature, extreme temperatures, either low or high, have not been shown to greatly affect strength. Low temperature (-28° C) was not found to significantly

affect bond between CFRP and concrete when tested on 1/3 scale beams (El-Hacha *et al.* 2004), although other studies found some deleterious effects in the form of matrix hardening and fiber-matrix bond degradation under subzero temperatures (Karbhari 2002). Karbhari *et al.* (2003) noted that high temperatures cause the resin or adhesive to soften excessively, creating a potential weakness. Remaining within the manufacturer's suggested service temperatures was recommended. Myers and Ekenel (2005) examined installation temperatures and established recommended limits based on strength and workability to be between 4°C and 32° C for the two FRP systems studied.

An extreme temperature fluctuation, or freeze/thaw cycling, is another parameter that has been investigated with conflicting findings for strength. A study by Bisby and Green (2002) reviewed the available literature and found some research indicated a decrease in overall strength as a result of exposure to freeze/thaw cycles while other studies showed no significant effect. Their research on 39 small-scale beam specimens supported the conclusion that the change in temperature extremes alone does not adversely affect the overall flexural strength of the specimen. An earlier study by Green *et al.* (2000) found similar results. Kong *et al.* (2005) recently showed that axial compressive strength of wrapped concrete cylinders was reduced only 3% as a result of cyclic thermal exposure. The bond of the FRP to the concrete was not affected by the cyclic exposure but there was a change in the adhesive properties as evidenced by a change in failure modes.

In contrast, del Mar Lopez *et al.* (1999) tested 48 small-scale beam specimens and found that the moment capacity and the maximum deflection decreased as a function of freeze/thaw cycles. It was also noted that precracked beams exhibited a larger decrease

than initially uncracked specimens. Saenz *et al.* (2004) found degradation of a range of FRP composite systems after 50 accelerated freeze/thaw cycles, although the thaw cycles were conducted in salt water. Grace (2004) found reductions in strength of 3.3% and 9.5% for beam specimens strengthened with CFRP plates subjected to 350 and 700 freeze-thaw cycles, respectively.

Moisture

Exposure to moisture alone has not been as well-researched because it is commonly coupled with other environmental effects such as temperature or various solutions. Grace (2004) found that 87% of the effectiveness of the CFRP strengthening scheme can be lost if the specimen is exposed to long-term relative humidity of 100%. Karbhari *et al.* (2003) gap analysis confirmed this finding showing that exposure to moisture can have deleterious effects on the fiber-matrix bond due to wicking along the interphase.

Sen *et al*. (2001) investigated the effects of moisture exposure combined with thermal changes for CFRP bonded to concrete slabs over a period of 17 months. Tensile and shear bond tests were performed after exposure and results indicated that wetting and drying produced lower strengths and addition of temperature cycling did not prove detrimental.

Wu *et al.* (2004) studied the effect of water on the cure and mechanical properties of epoxy adhesives. They found that a small amount of water (+2%) improved the cure time and the modulus and strength properties but excess water (> +4%) had a negative impact on these same properties.

Shear Fatigue of CFRP Strengthened Members

Previous laboratory investigation (Higgins *et al*. 2006) involving fatigue response of externally bonded FRP laminates studied full-scale girders, replicated to the existing conditions of typical 1950`s vintage RCDG bridges. Loading conditions for the tests were established from measurements of in-situ CFRP strain data under ambient traffic conditions over a period of 30 days. Service-level fatigue loading, accelerated to simulate extended service life, was found to not change the ultimate capacity of the specimens. However, cyclic loading test showed that the interface debonding propagates progressively with increase of the fatigue cycles. Interface debonding areas may accelerate in the presence of combined fatigue and freeze-thaw exposures.

Synergistic Effects

Karbhari *et al.* (2003) conducted a comprehensive durability gap analysis and one of the main conclusions was the need for examination of combined effects. In-situ FRP installations do not have just one of these environmental conditions in isolation, so further studies under more realistic combined conditions was recommended.

Some durability studies have already examined the effects from combinations of environmental conditions. Malavar *et al.* (2003) found that the combination of high humidity and high temperature had a large impact on the bond strength as measured by pull-off tests. Maximum relative humidity during adhesive application was recommended to be 85%, which was later confirmed by research done by Myers and Ekenel (2005).

Mukhopadhyaya *et al.* (1998) found that bond transfer length, shear stress, and plate slip increased with freeze/thaw and wet/dry cycles using a chloride solution as well as with a combination of the two. However, ultimate strength did not appear to be effected and this was attributed to the accelerated nature of the tests. Exposure duration was only for 9 months but it was predicted that these effects would become more significant over an extended period of time.

CFRP Design Provisions for Environmental Exposure

Design provisions for FRP strengthening of RC structures have been developed by the American Concrete Institute Committee 440 (ACI 440.2R-08). These provisions include strength reduction factors to account for environmental exposure conditions. ACI-440 provides a list of possible environmental exposure conditions that may impact performance including salt water, high temperatures, high humidity, and freezing and thawing cycles.

The current approach is to adjust the FRP material ultimate tensile strength, f_{fu}^*, and the ultimate rupture strain, ε_{fu}^* with an environmental-reduction factor, C_E, as:

$$f_{fu} = C_E f_{fu}^* \qquad \text{(ACI-440 Eqn 8-3)} \quad [1]$$

$$\varepsilon_{fu} = C_E \varepsilon_{fu}^* \qquad \text{(ACI-440 Eqn 8-4)} \quad [2]$$

to produce the design ultimate tensile strength, f_{fu}, and design rupture strain, ε_{fu}. The environmental-reduction factors depend on the exposure condition and the type of FRP material as shown in Table 2.1. As this table shows, if the FRP system is located in a relatively mild environment, the reduction factors are close to unity.

Table 2.1 - ACI-440 Table 8.1 Reduction factors for various FRP systems subjected to environmental exposure conditions

Exposure Conditions	Fiber and Resin Type	Environmental-reduction factor C_E
Interior Exposure	Carbon/epoxy	0.95
	Glass/epoxy	0.75
	Aramid/epoxy	0.85
Exterior exposure (bridges, piers, and unenclosed parking garages)	Carbon/epoxy	0.85
	Glass/epoxy	0.65
	Aramid/epoxy	0.75
Aggressive environment (chemical plants and waste water treatment plants)	Carbon/epoxy	0.85
	Glass/epoxy	0.50
	Aramid/epoxy	0.70

The above modification to the FRP material design properties is the only means employed in ACI-440 to reflect the effects of environmental exposure on FRP strength. Currently, there is no reduction taken directly for bond strength based on environmental exposure. Bond reduction coefficients are based on the wrap configuration and compressive concrete strength, and are used to further reduce the design rupture strain to produce an effective strain. The maximum effective strain is limited at 0.4% (0.004 in/in). In practice, when using the current approach, the reduced manufacturer-specified ultimate rupture strain (accounting for environmental exposure, wrap configuration, and compressive concrete strength) often still results in an effective strain greater than 0.4%. As a result, the effective strain for design is limited to 0.4% and in effect, the environmental exposure may not be adequately captured if it has a deleterious effect on the bond properties.

Summary

The additional strength provided by CFRP materials depends principally on the bond between the member substrate and the CFRP, which allows stress transfer from the

concrete component to CFRP laminate. For most common shear strengthening applications, the member strength is governed by debonding of the CFRP strips and thus the material strength cannot be fully utilized. The causes and mechanisms of bond failure are complex, and past research has shown conflicting results related to the effects of different environmental exposures. Very limited previous work has been conducted related to CFRP for shear strengthening and a need exists to quantify the effects of environmental exposure on structural performance of CFRP shear-strengthened members, and identify possible negative consequences of combined high-cycle fatigue and environmental exposure.

The objectives of this research are to:

1) Develop realistic full-size specimens, apply CFRP reinforcement, and subject to accelerated environmental exposures. Exposures to be considered include freeze-thaw, freeze-thaw combined with high-cycle fatigue, and water immersion.
2) Experimentally determine the effects of the environmental exposures on the structural performance of the CFRP shear-strengthened members by comparing with similar unexposed specimens.
3) Analytically predict the shear strength of the CFRP strengthened specimens and quantitatively estimate the effects of the environmental exposures.
4) Report experimental and analytical findings and make recommendations for CFRP strengthening applications that are exposed to long-term environmental exposures.

3 RESEARCH SIGNIFICANCE

Long-term durability of surface-bonded CFRP for strengthening reinforced concrete bridge members remains uncertain due to the limited field experience with these materials. The possible long-term durability issues are the structural performance of CFRP strengthened members under moisture and freeze-thaw as well as combined with high-cycle fatigue loading. Past experimental research on environmental durability has been limited to reduced-scale specimens and focused primarily on flexural reinforcing and bond strength. The influence of both environmental conditioning and structural performance of CFRP materials on small scale samples is not well understood and extrapolation to full-scale performance is uncertain. No information is available regarding shear strengthening applications and the effect of environmental exposure in shear dominant regions. Previous research investigated environmental exposure for applications without previous cracking of the base concrete that may have an impact on the durability due to water moving through the material at those locations. The orientation of the specimen is also important consideration for environmental durability. The current research avoids these issues by testing structural performance of full-scale RC bridge girder specimens strengthened for shear after extended environmental exposures. A test protocol was developed for environmental exposure cycling and the experimental results provide new information on long-term durability of CFRP under these conditions.

4 EXPERIMENTAL PROGRAM

To investigate the effects of environmental durability and combined action of cyclic loading + environment on the structural performance of reinforced concrete bridge girders strengthened for shear with surface-bonded CFRP, an experimental program was undertaken. The general testing procedure consisted of the following steps:

i. Imposition of initial diagonal and flexural cracking in the RC specimens (defined here as precracking).
ii. Epoxy injection of diagonal cracks.
iii. Preparation of concrete surfaces.
iv. Installation of CFRP materials.
v. Reloading of CFRP strengthened beam to reproduce diagonal cracking (defined here as recracking)
vi. Development and application of a environmental exposure protocol (combined with high-cycle fatigue load cycles for specimen FFT18CK)
vii. Structural testing to failure.

To examine the bond properties of different CFRP materials subjected to same environmental exposure protocol, a separate test matrix and sequence was implemented. The above points are subsequently described in the sections below.

4.1 Test Specimens

Four full-scale reinforced concrete girders were constructed, representative of 1950's vintage proportions and detailing, for conventionally reinforced concrete deck girders found in highway bridges [Higgins *et al.* 2004]. The specimens consisted of one T and three inverted-T (IT) beams which were designed to fail in shear with typically

encountered flexural steel proportions to provide realistic shear-moment interaction. The T configuration represents shear in the presence of positive moment, as near abutment locations, and the IT configuration represents shear in the presence of negative moment, as near continuous support locations. The specimens had an overall stem height of 1219 mm (48 in.), a web thickness of 356 mm (14 in.), a flange thickness of 152 mm (6 in.), and a flange width of 914 mm (36 in.) and are illustrated in Figs. 4.1 and 4.2. The flexural steel for both T and IT specimens consisted of well anchored #36 (#11) bars that enable development of the bar yield stress at diagonal crack locations within the span.

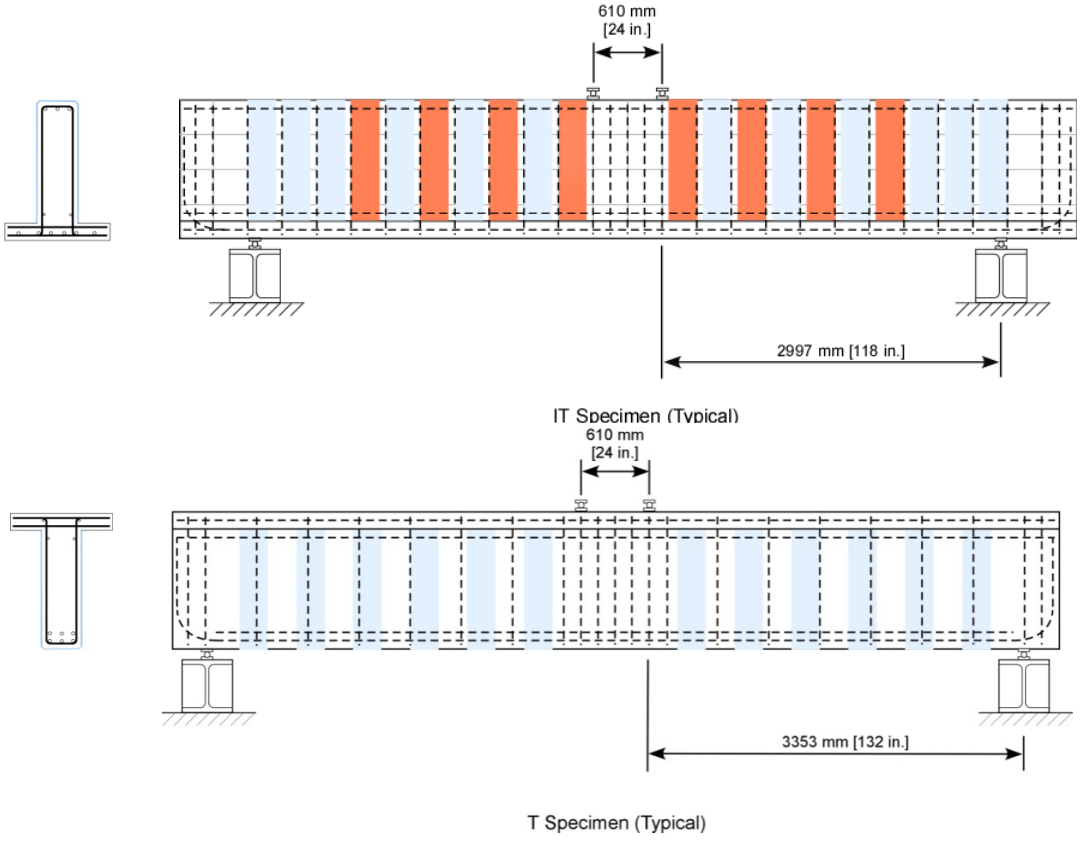

Fig. 4.1 – Typical inverted-T and T specimen elevation views.

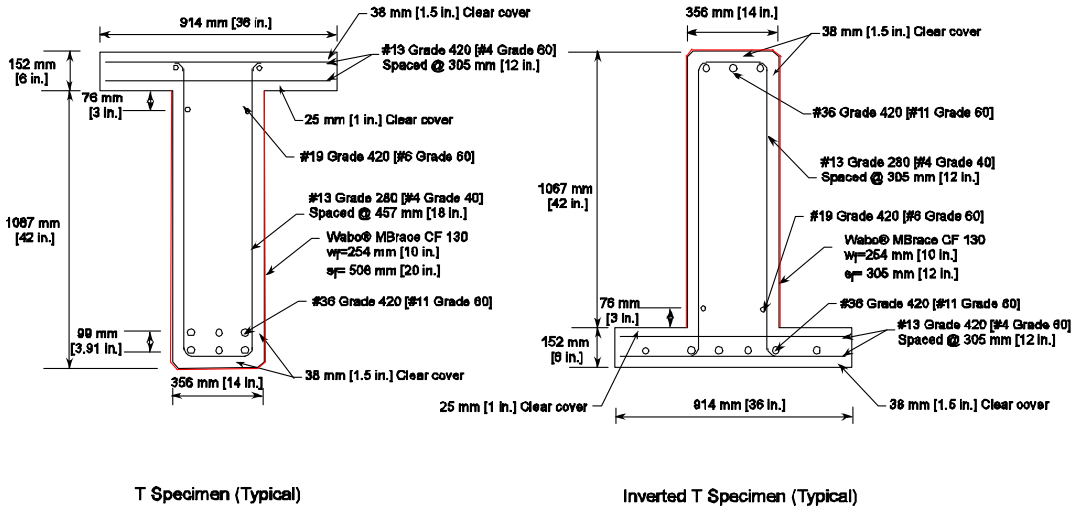

Fig. 4.2 – Typical T and inverted-T specimen section views.

4.2 Materials

Concrete was provided by a local ready-mix supplier for all specimens. The concrete mix design was based on 1950's AASHO "Class A" concrete used in previous research at OSU [Higgins *et al.* 2004]. The aggregate composition for the mix was reported by the supplier as: 97% passing the 19 mm sieve (3/4 in.), 82% passing 16 mm (5/8 in.), 57% passing 12.5 mm (1/2 in.), 33% passing 9.5 mm (3/8 in.), 21% passing 8 mm (5/16 in.), 9.3% passing 6.3 mm (1/4 in.), 3.0% passing 4.75 mm (#4), 0.6% passing 2.36 mm (#8) and 0.3% passing the 0.075 mm (#200) sieve. The sand composition of the mix was also reported as: 99.7% passing the 6.3 mm sieve (1/4 in.), 96.8% passing 2.36 mm (#8), 59.4% passing 1.18 mm (#16), 44.9% passing 0.600 mm (#30), 17.9% passing 0.300 mm (#50), 3.7% passing 0.150 mm (#100) and 1.7% passing the 0.075 mm (#200) sieve. The coarse aggregate was from Willamette River bed deposits consisting of smooth rounded basaltic rock. Specified compressive strength was 21 MPa (3000 psi), which is comparable to the

specified design strength in the original 1950's bridges. Actual concrete compressive strengths were determined from 152 x 305 mm (6 in. x 12 in.) cylinders tested for 28-day and day-of-test strengths in accordance with ASTM C39M/C 39M-05 and ASTM C617-05. Concrete cylinder strengths for each specimen are shown in Table 4.1.

Longitudinal steel was #36 ASTM A615 Grade 420 (#11 Grade 60) bars while transverse steel was #13 ASTM A615 Grade 280 (#4 Grade 40) open stirrups. Actual steel reinforcing properties were determined from tensile tests per ASTM A 370 and ASTM E 8. Three 406 mm (16 in.) long samples were cut from the #13 (#4) bars while three coupons were made for the #36 (#11) bars according to the above ASTM standards. Tensile specimens were tested with a 489 kN (110 kip) universal testing machine with constant head speeds of 0.0169 mm/sec (0.000667 in./sec) for #13 (#4) and #36 (#11) bars.

Table 4.1: Concrete cylinder strengths.

Specimen	28-day	Precrack		Recrack		Failure	
	f'_c (MPa) [psi]	f'_c (MPa) [psi]	f_t (MPa) [psi]	f'_c (MPa) [psi]	f_t (MPa) [psi]	f'_c (MPa) [psi]	f_t (MPa) [psi]
IT12Control	27.6 [4008]	31.0 [4498]	2.74 [398]	N/A	N/A	31.8 [4606]	2.93 [425]
T18Control	26.9 [3900]	30.1 [4372]	2.95 [427]	N/A	N/A	29.8 [4329]	2.93 [425]
IT12M	30.03 [4356]	32.92 [4776]	3.42 [497]	N/A	N/A	33.18 [4813]	3.6 [523]
IT12MCK	28.35 [4112]	29.21 [4237]	3.54 [513]	29.75 [4314]	N/A	30.4 [4409]	3.84 [557]
ITT12FTCK	25.26 [3664]	24.7 [3583]	2.9 [422]	24.3 [3526]	N/A	22.74 [3298]	2.4 [353]
FFT18CK	31 [4496]	28.94 [4197]	3.98 [577]	29.45 [4272]	N/A	28.34 [4112]	2.8 [404]
Bond Specimens	26.9 [3900]	30.1 [4372]	2.95 [427]	N/A	N/A	29.8 [4329]	2.93 [425]

Strain was measured using a class B1 extensometer with 50 mm (2 in.) gage length. Measured mean steel properties are given in Table 4.2.

Table 4.2: Mean reinforcing steel properties.

Specimens	Material	Bar Size (mm) [in.]	Grade (MPa) [ksi]	f_y (MPa) [ksi]	f_{ult} (MPa) [ksi]
IT12M IT12MCK	Flexural Steel	#36 [#11]	A615 Gr. 420 [Gr. 60]	466 [67.6]	784 [113.7]
ITT12FTCK FFT18CK				491.5 [71.3]	827 [119.9]

For CFRP material properties, a 610 mm x 610 mm (24 in. x 24 in.) sheet of CFRP was prepared as part of the installation process done on the specimens. One coat of saturant was rolled onto a Teflon board, carbon fiber fabric was placed and saturated with the base saturant, and a final coat of saturant was added before placing another Teflon board on top. These sample sheets were cured under the same temperature conditions as the specimens. After curing, 25 mm x 305 mm (1 in. x 12 in.) coupons were cut from the sheet using a wet tile saw. Care was taken to ensure cuts were oriented along the fiber direction. The coupons were prepared and tested in accordance with ASTM D 3039. Perforated fiberglass programming board tabs 25 mm x 57 mm (1 in. x 2.25 in.) were cut and attached to the ends of the CFRP coupons with cyanoacrolyte adhesive to prevent crushing of the CFRP in the grips of the tensile testing machine. Coupons were tested using a 89kN (20 kip) universal testing machine with a constant head speed of 1.25 mm/min (0.05 in./min) and strains were measured using a Class B extensometer with a 25 mm (1 in.) gage length.

Direct pull-off tension tests of the CFRP were also completed for each specimen in accordance with ASTM D 4541. After failure testing of specimens, four undisturbed

regions of CFRP were prepared and cleaned before applying a 51 mm x 51 mm (2 in. x 2 in.) steel square dolly with adhesive. The surface is first roughened with the sand paper so that the square dolly would bond well to the CFRP. The adhesive was allowed to cure before using an abrasive cutting wheel to cut the CFRP around the edges of the dolly so as to make the surface contact area 4 sq. in. A 1.6 kN (3600 lb) capacity portable testing device with digital manometer was used to pull and record the maximum load. The mean and standard deviation of the tension pull-off strengths for each specimen and for different CFRP systems are shown in Table 4.3 and Table 4.4.

Table 4.3: CFRP pull-off tensile strengths.

Specimen	Mean $f_{pull\text{-}off}$ (MPa) [psi]	Standard Deviation $f_{pull\text{-}off}$ (MPa) [psi]
IT12Control	2.45 [355]	0.53 [76.52]
T18Control	2.70 [391]	0.80 [115.64]
IT12M	3.06 [445]	0.94 [136]
IT12MCK	2.60 [377]	1.06 [154.75]
ITT12FTCK	2.84 [413]	0.84 [122.75]
T18FFTCK	2.40 [349]	1.51 [219.10]

Table 4.4: Pull-off tensile strengths for Different CFRP systems.

CFRP System	Control		Freeze-Thaw	
	Mean $f_{pull\text{-}off}$ (MPa) [psi]	Standard Deviation $f_{pull\text{-}off}$ (MPa) [psi]	Mean $f_{pull\text{-}off}$ (MPa) [psi]	Standard Deviation $f_{pull\text{-}off}$ (MPa) [psi]
Edge	2.63 [383]	0.26 [38]	2.48 [360]	0.7 [100]
Fyfe	2.5 [361]	0.75[109]	2.53 [367]	0.21[31]
Sika	2.04 [293]	0.35 [51]	2.3 [334]	0.25[36]

Failure occurred for all tests in the concrete substrate. Pull off tests were also done on the exposed concrete surface. The mean and standard deviation of the tension pull-off strengths for concrete are shown in Table 4.5.

Table 4.5: Concrete pull-off tensile strengths.

Specimen	Mean $f_{pull\text{-}off}$ (MPa) [psi]	Standard Deviation $f_{pull\text{-}off}$ (MPa) [psi]
Control	2.15 [312.5]	0.25 [37.5]
Moisture Specimens	2.84 [412.5]	0.33 [49]
Freeze Thaw Specimens	2.71 [393.4]	0.56 [81.75]

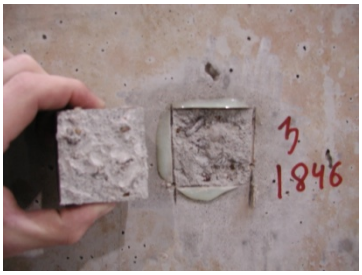

4.3 Test Setup

The experimental program consisted of 4 specimens, which were compared with the control specimens, listed in Table 4.6. Three were tested in the IT configuration and one tested in the T configuration. To characterize the performance of the CFRP strengthened specimens independent of the environmental exposure, two otherwise identical control specimens were tested as part of a prior study (Mitchell 2008): one in the IT configuration, and one in the T configuration. Out of three IT specimens, two were tested for moisture exposure, one of which was reloaded to produce diagonal cracks after the CFRP material was applied and prior to moisture exposure. The remaining IT and T specimens were subjected to environmental freeze-thaw exposure, which were also loaded to produce diagonal cracks after the CFRP material was applied. The specimen age at key points in the test program are shown in Table 4.7. All specimens were initially precracked and strengthened with the same epoxy and CFRP materials. All specimens produced first

diagonal cracking at shear of approximately 137kN (31 kips). Initial cracking for the specimens (called precracking in this study) was done by subjecting the initial RC beam to a maximum shear of 667 kN (150 kips) for the IT and 556 kN (125 kip) for the T specimens. These forces correspond to about 90% and 83% of the ultimate capacity as predicted by Response-2000 [Bentz 2001] for the IT and T specimens, respectively. The maximum diagonal crack widths under load at these stages were 1.52 mm (0.06 in.) for the IT specimens and 1.78 mm (0.07 in.) for the T specimens.

After initial cracking, a baseline test was performed to evaluate the stiffness, deformations, and stresses of the cracked beams. The precracked condition for all specimens is shown in Fig. 4.3. Epoxy injection of the injectable diagonal cracks was performed and the CFRP applied before each of the specimen configurations was then recracked by applying 1001 kN (225 kips) and 725 kN (163 kips) of shear to the IT and T beams, respectively. Similar to the initial precracking phase, a second baseline test was performed to evaluate the stiffness, deformations, and stresses of the recracked CFRP strengthened beams.

Table 4.6: Experimental program.

Specimen	Type	Precrack Shear (kN) [kip]	Recrack Shear (kN) [kip]	Freeze-Thaw (cycles)	Moisture Exposure (Time in Months)
IT12Control	IT	667 [150]	N/A	N/A	N/A
T18Control	T	556 [125]	N/A	N/A	N/A
IT12M	IT	667 [150]	N/A	N/A	6
IT12MCK	IT	667 [150]	890[200]	N/A	6
ITT12FTCK	IT	667 [150]	1001[225]	300	N/A
T18FFTCK	T	556 [125]	729[163]	300	N/A

Table 4.7: Specimen cast dates and testing ages.

Specimen	Cast Date	Age at Precrack (Days)	Age at Recrack (Days)	Age at F-T Start (Days)	Age at Failure (Days)
IT12Control	3/4/08	43	N/A	N/A	71
T18Control	3/4/08	48	N/A	N/A	69
IT12M	09/07/07	104	N/A	N/A	389
IT12MCK	09/07/07	110	149	N/A	385
ITT12FTCK	04/30/08	58	72	78	191
FFT18CK	04/30/08	57	71	78	197

The specimens named with “CK” are the ones which were recracked after installation of the CFRP. The recracked condition for all specimens is shown in Fig. 4.4. Both the recracked and undisturbed CFRP strengthened specimens were then subjected to same environmental exposure and finally tested to ultimate. The specimens IT12MCK and IT12M were kept submerged in water for 234 days. Specimens ITT12MCK and FFT18CK were subjected to freeze-thaw exposure together.

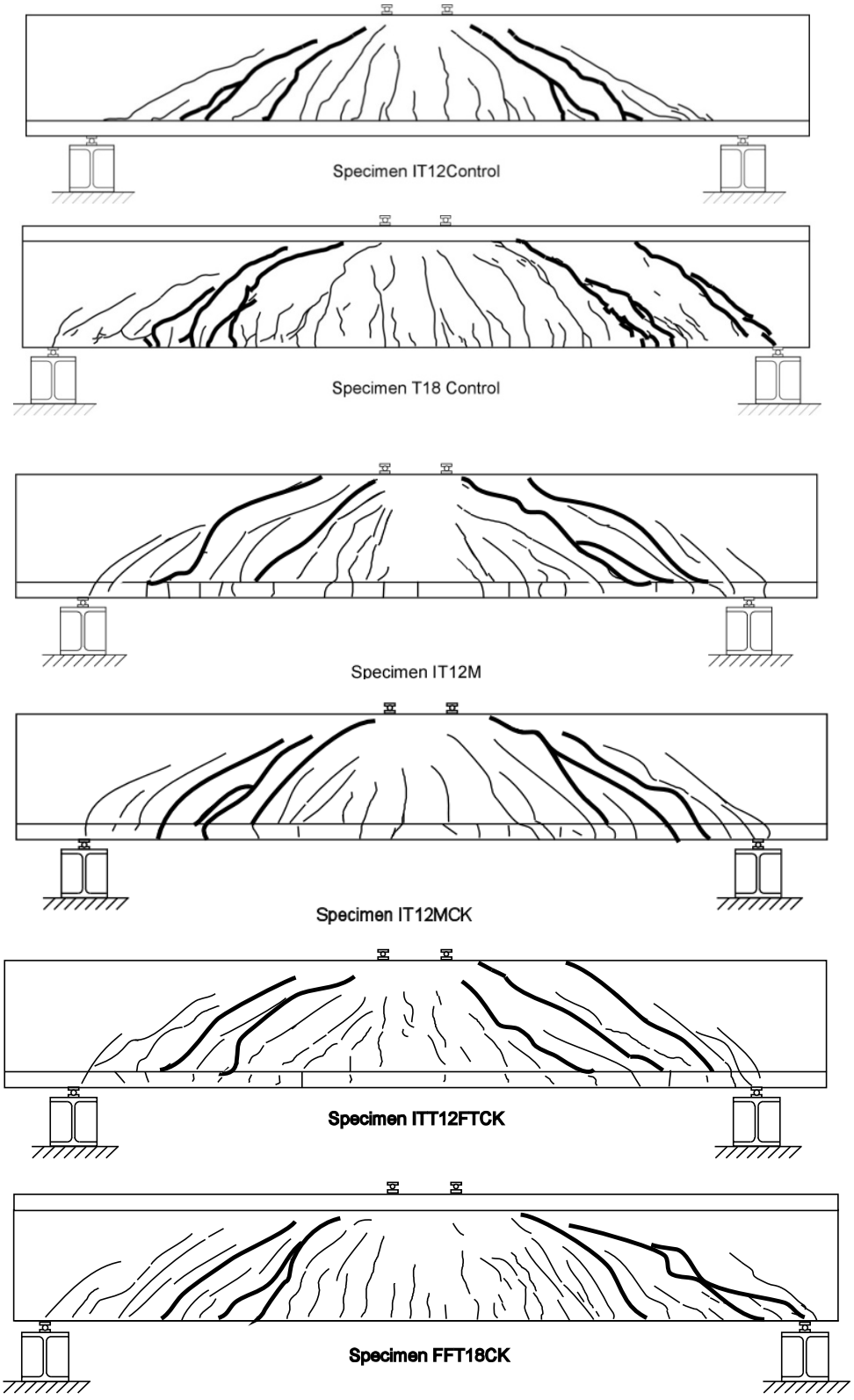

Figure 4.3 – Precracked condition of all specimens.

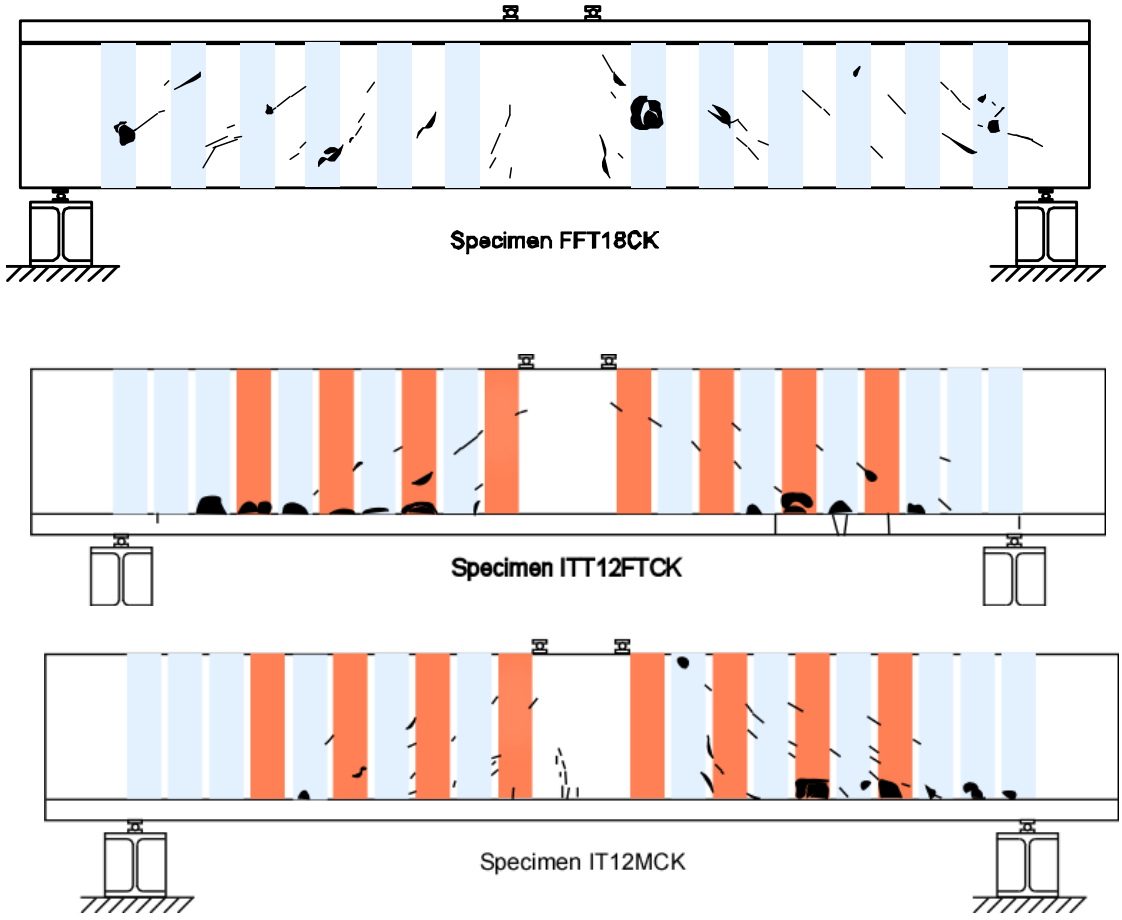

Figure 4.4 – Recracked condition of all specimens

4.4 Structural Testing

Specimens were subjected to the precrack, recrack, and failure tests on the strong floor at the Structural Engineering Research Laboratory at Oregon State University. The specimens were tested in a simply supported configuration under four-point loading. The typical loading setup is shown in Fig. 4.5.

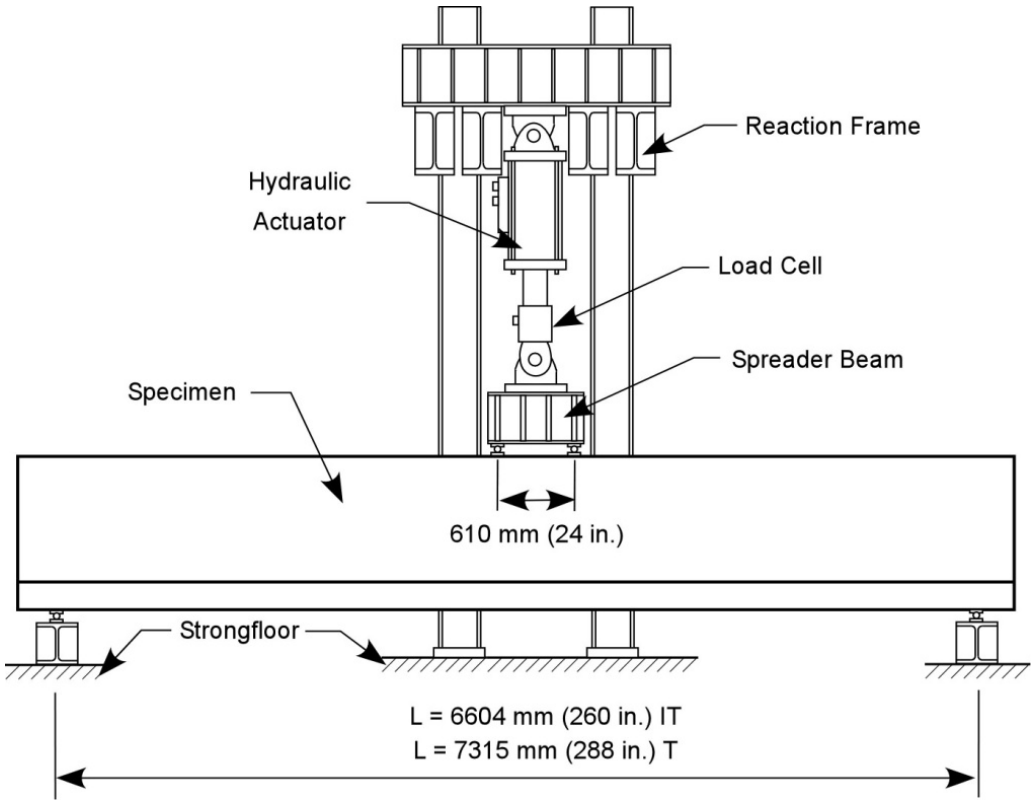

Fig. 4.5 – Typical static load setup.

IT specimens were loaded on a 6604 mm (260 in.) overall span while T specimens were loaded on a 7315 mm (288 in.) overall span. The specimens were supported on 102 mm (4 in.) wide bearing plates resting on 51 mm (2 in.) diameter rollers. Load was applied at midspan to 51 mm (2 in.) rollers resting on 102 mm (4 in.) wide bearing plates through a spreader beam with a 610 mm (24 in.) span. Loads were measured with a 2224 kN (500

kip) capacity load cell and applied using a hydraulic actuator at a rate of 9 kN/sec. (2 kip/sec.). All tests included several load cycles; with the applied load increasing 222 kN (50 kip) for each cycle. For each cycle, once the target load amplitude was achieved, it was immediately decreased by 10% to permit identification of visible cracks and debonding, and then the specimen was unloaded to continue on to the next loading sequence. Debonding of the CFRP was identified by tapping on the surface and listening for a distinct hollow sound. Additionally, a FLIR infrared camera was used to identify debonding. A halogen light was passed across regions of suspected debonding and a thermographic image was taken. Debonded regions did not dissipate the heat quickly and appeared warmer on the thermographic image. A correlation of a debonded region identified by the tapping method with the thermographic image is shown in Fig. 4.6.

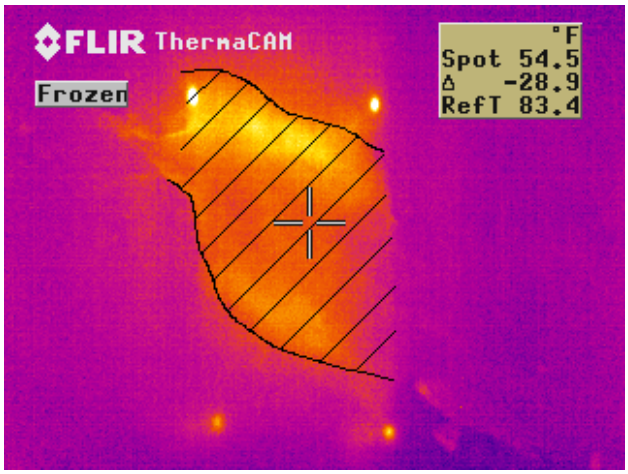

Fig. 4.6 – Thermographic image of debonding

Fatigue loading was conducted for specimen T18FFTCK using a sinusoidal loading function with unique load ranges to obtain target damage using one million applied load cycles. A 1334 kN (300 kip) capacity load cell was used for feedback of the load control

protocol and load was applied with a 978 kN (220 kip) capacity actuator. The T specimen FFT18CK was fatigued at a load range of 267 kN (60 kips) with a mean of 445 kN (100 kips) at a frequency of 1.00 Hz. Every day 25,000 cycles were completed and the hydraulic system was turned off at it the end of each day. The applied load coincided with simultaneous freeze-thaw cycles. Load was applied at midspan on a steel plate size 256 mm (14 in.) x 256 mm (14 in.). Before starting the actual load cycles, a baseline test was conducted because the shear span of the beam in environmental chamber was slightly larger due to the single point load. After every 100,000 cycles a baseline test was conducted to check the stiffness and overall deflection. After the baseline test, both the specimens in the freezer were inspected for cracks and CFRP debonding. A schematic presentation of loading setup in freezer is shown in Fig. 4.7 and Fig. 4.8.

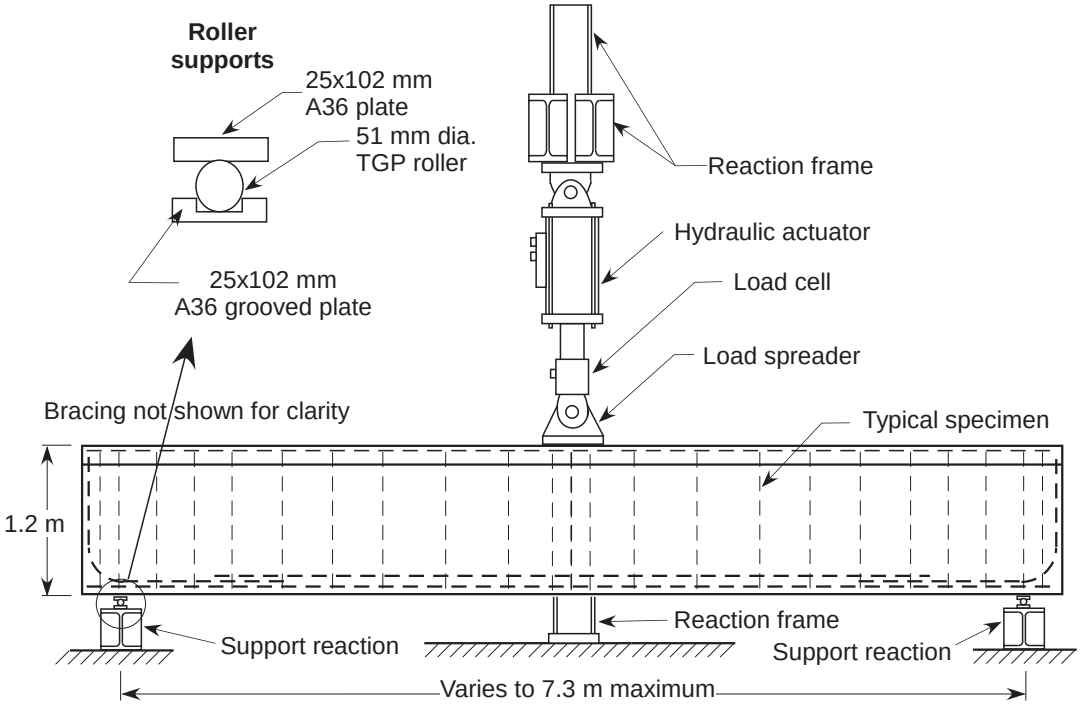

Fig. 4.7 Fatigue + Freeze-Thaw Loading Setup (Side View)

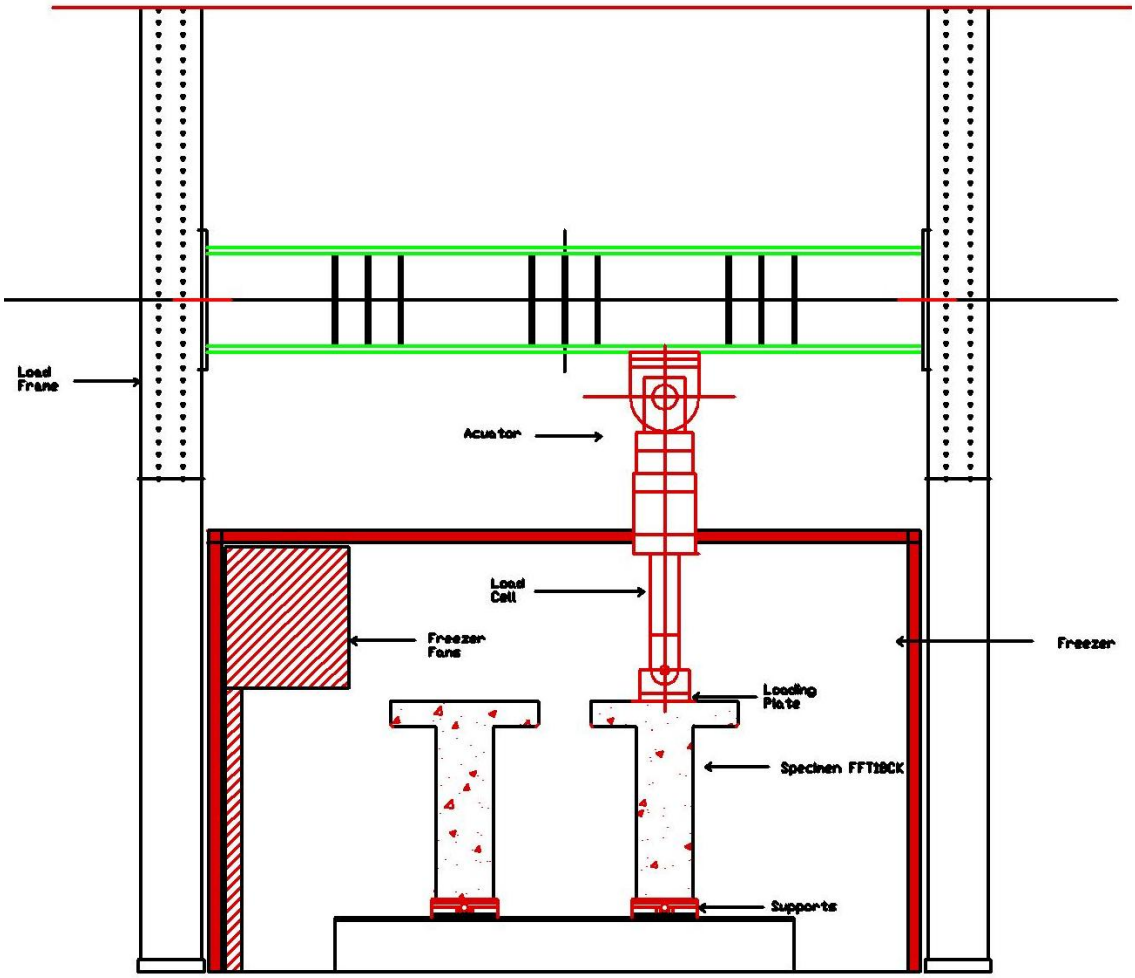

Fig. 4.8 Fatigue + Freeze-Thaw Loading Setup (South View)

4.5 Instrumentation

Instruments were applied to the specimens to measure overall and local deformations, CFRP and reinforcing steel strains, support motions, and applied force. Typical instrumentation layout used for all specimens is illustrated in Fig. 4.9. Transverse steel strains were measured locally at midheight of the specimen while longitudinal rebar strains were measured at midspan. Steel strains were measured using short gage length CEA-06-125UN-120 strain gages to minimize the locally debonded region around the sensors. Local CFRP strains were measured at expected diagonal crack locations using either N2A-06-20CBW-120 or EA-06-20CBW-120. These gages had a 51 mm (2 in.) length allowing for the strains to be averaged over multiple CFRP weaves. Diagonal deformations were measured with 51 mm (2 in.) string potentiometers, to permit average strains to be

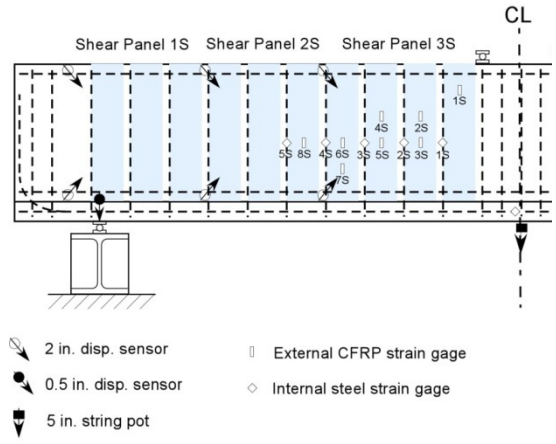

Fig. 4.9 – Typical instrumentation layout for all specimens.

calculated over three regions on each shear span. Midspan displacements were measured using 127 mm (5 in.) string potentiometers while support settlements were measured using 13 mm (0.5 in.) range displacement sensors. Support deformations were subtracted from

midspan displacements so rigid body displacements were removed from the reported overall midspan displacement of the specimens.

Three N2A-06-20CBW-120 gauges were installed along the CFRP plates of prism to measure the distribution of strain. Midspan displacement was measured using 13 mm (0.5 in.) range displacement sensors to compare the stiffness. For specimen T18FFTCK, care was taken so that the baseline tests were always done during warm temperature cycles in the freezer. All the diagonal sensors and displacement gauges were mounted on the specimen and removed after the baseline tests to protect from moisture damage. All the internal steel strain gauges and external CFRP gauges remained connected to record strain data at 0.1 Hz frequency.

4.6 CFRP Installation

After precracking, the load was removed from the specimens and the unidirectional CFRP U-wraps were applied using a wet lay-up procedure. Application was performed according to the manufacturer's specifications [Watson Bowman Acme 2002] and is described below.

4.6.1 Epoxy Injection

Cracks wider than 0.25 mm (0.010 in.) were epoxy injected using Chemrex SCB Concresive 1360. The concrete surface around the diagonal cracks was cleaned and the cracks were sealed and injection ports were placed at the crack surface. Concresive SPL paste was used to seal the cracks at the concrete surface. On one side of the web, injection ports were installed at a spacing of approximately 356 mm (14 in.), while only three

injection ports were placed on the opposite side of the web. One port was placed at the bottom of the web, one at mid-height, and one near the top. The surface sealant was allowed to cure for 24 hrs before injection. An epoxy injection machine with mixing nozzle was used, allowing for the proper proportioning and mixing of the two-part epoxy. The machine also provided pressure readings during injection. The injection nozzle was placed at the bottom-most port and the injection pressure kept below 0.69 MPa (100 psi) until epoxy was visible in the port above. The lower port was capped and the injection nozzle moved to the next port. Window ports on the opposite side of the web were monitored to ensure epoxy was flowing through the thickness of the web. Injection continued from the bottom to the top of the specimen until the top-most port was reached. Epoxy was injected at this port until a pressure of 0.69 MPa (100 psi) could be maintained. The epoxy was allowed to cure for at least 7 days at temperature above 4°C (40°F) before the next application step. Injected cracks are shown in bold in Fig. 4.3.

4.6.2 CFRP Application MBrace system

After epoxy injection, the surface was prepared for CFRP application. First, the surface crack sealing paste was removed by heating and scraping it off. Next, the surface was ground using a diamond dressed masonry disc, removing the concrete paste surface to expose aggregate and small voids. Additionally, all sharp edges were rounded using the masonry disc. Finally, the surface was vacuumed to remove dust that had accumulated during grinding. Once the surface preparation was completed, the CFRP system was installed. First the two-part MBrace Primer was mixed with a mechanical mixer for 3 minutes and applied to the concrete surface using nap rollers with a coverage rate of approximately 3.8-4.9 m^2/L (150-200 ft^2/gal). The primer was allowed to cure for several

hours before the two-part MBrace putty was applied. Part A of the putty was premixed for 3 minutes, as was Part B. Part A was then added to Part B and mixed for 3 minutes. This was then applied using trowels to fill small voids and smooth small imperfections in the concrete surface. Finally, the two-part MBrace saturant was mixed. Part A was premixed for 3 minutes, Part B was added and then the combined elements were mixed for an additional 3 minutes. This was then rolled on to the surface with a thickness of approximately 0.46-0.51 mm (18-20 mil) corresponding to a coverage rate of approximately 1.3 m^2/L (35-55 ft^2/gal). Strips of dry MBrace CF130 carbon fiber fabric were then applied while the saturant was still wet. A plastic putty knife, running in the direction of the fibers, was used to press the fabric into the saturant, impregnating the fabric and removing all air bubbles. A final coat of MBrace saturant was rolled over the fabric with the same thickness and coverage rate as the first coat. As learned from previous repairs, for Freeze-Thaw specimens, care was taken that CFRP strips ending at the edges of the beams were fully saturated with the resin and more resin was intentionally used to seal the nearby area to protect it against moisture. The specimen was then cured for at least 7 days in a heated enclosure to ensure the ambient temperature remained above 4°C (40°F). Average 7 day curing temperatures for each application are shown in Table 4.8. After the saturant set up, it was scuffed with sandpaper and vacuumed to permit application of the topcoat. The MBrace Topcoat ATX was mixed for 3 minutes with a mechanical mixer then rolled on with a coverage rate of approximately 1.94-2.43 m^2/L (80 to 100 ft^2/gal) using a nap roller.

Table 4.8: Average 7 day curing temperatures.

Specimen	Average Curing Temperature (°C) [°F]
IT12Control	17 [62]
T18Control	17 [62]
IT12M	8 [48]
IT12MCK	8 [48]
ITT12FTCK	22[73]
FFT18CK	22[73]

4.7 Environmental Exposure

4.7.1 Moisture Specimens

Two full scale specimens, IT12M and IT12MCK, were kept submerged under water for six months in a bath tub. A tub with length 8180 mm (322 in.), width 2413 mm (95 in.) and height 1372 mm (54 in.) was constructed using plywood and dimensional lumber. A pond liner was placed inside the tank to hold the water. Treaded rod was used at the top and bottom along the long walls of tub to resist the hydrostatic pressure in the tub and 12.7 mm (0.5 in.) bolts were used to connect the corners of the wall. During the exposure, the water level in the tank was maintained above the level of the specimens. To monitor the water temperature, two thermocouples were installed to measure water and air temperatures around and in the tank. The statistical temperature data measured during the exposure are shown in Table 4.9. A schematic representation of tank is shown in Fig. 4.11 below with a photo of the specimens inside the tank. Air and moisture temperatures around the bathtub are shown in Fig. 4.12.

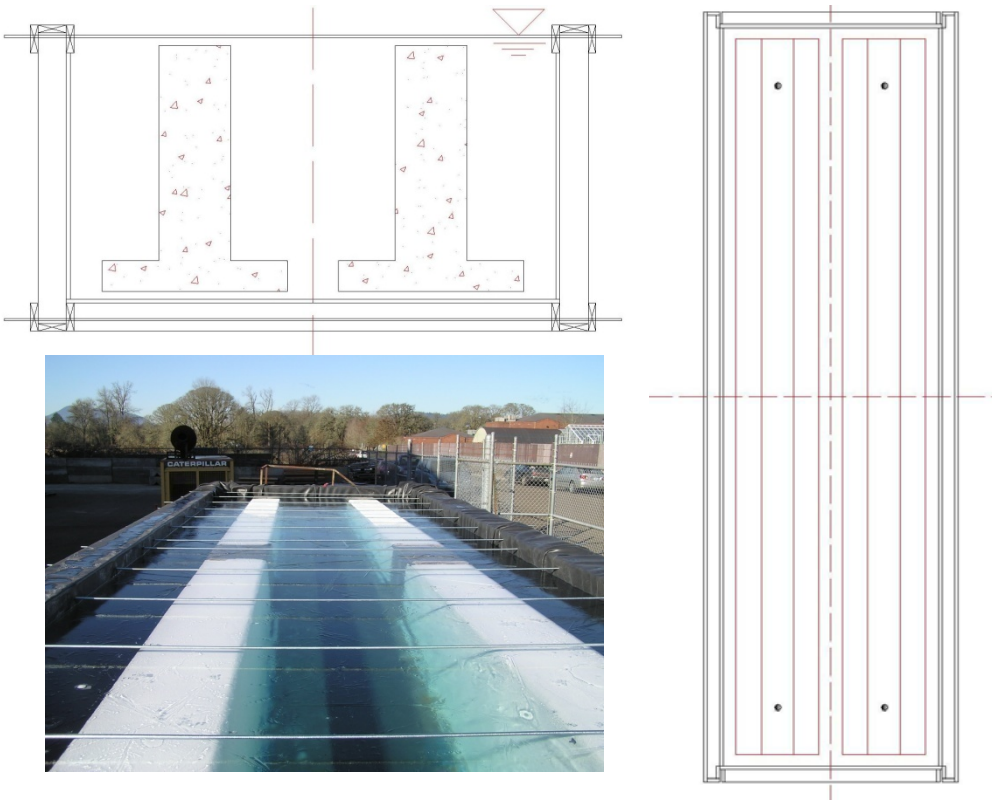

Fig. 4.10 Section, Elevation and actual picture of bathtub

Table 4.9 Air and Water Temperature data recorded over six months exposure.

Environment	Average Temperature (°C) [°F]
Air	17 [62]
Water	15 [59]

4.7.2 Freeze-Thaw specimens

Previous freeze-thaw exposure (Mitchell 2007) showed that more moisture was able to infiltrate specimens in the T configuration as compared with IT configuration because the CFRP application acted as a water resistant shell. Moisture, percolating through cracks in the T member orientation due to gravity collected behind the CFRP and repeated freezing and thawing led to reduced member strength. Learning from this prior result, it was decided to test IT specimen in the freezer in the T configuration. Along with environmental

exposure, a separate T specimen was subjected to additional fatigue loading conditions similar to previous laboratory experiments (Higgins *et al*. 2006) involving fatigue response of surface-bonded CFRP. Freezing and thawing of the specimens was achieved by cycling the ambient air temperature with a one-hour soak at -16°C (3°F), a 30 minute ramp to 16°C (61°F), a one hour soak at 16°C (61°F), and a 30 minute ramp back to -16°C (3°F). This ensured that the outer 13 mm (0.5 in.) of the specimen was thoroughly frozen and thawed during each cycle. This area was of interest and targeted for freeze-thaw because CFRP used in bond-critical applications, such as U-wrapped shear applications, must rely on stress transfer through the epoxy into the underlying concrete substrate. Each of these specimens was subjected to 300 freeze-thaw cycles. Temperatures in the environmental enclosure were measured using Type T thermocouples. The chamber air temperatures were measured at both ends of the specimen, the specimen surface temperature and internal temperature 51 mm (2 in.) from the surface were measured at midspan. Typical temperature cycling during the freeze-thaw conditioning at all four temperature measurement locations for a specimen is shown in Figure 4.12. The number of freeze-thaw cycles chosen for the test protocol was based on review of existing ASTM standards and by calculating expected freeze-thaw cycles for various regions in Oregon (Mitchell 2008). The 300 cycle threshold is meant as a reference measure and can be calibrated to actual exposure times in-situ based on heat transfer analysis of available local temperature records at the bridge site of interest for the given girder proportions.

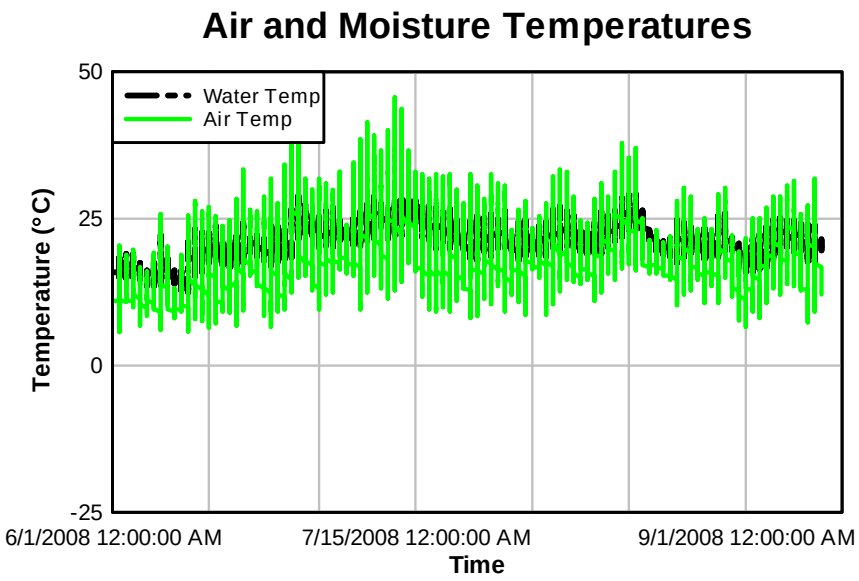

Fig. 4.11 Typical Temperature cycles for Bathtub

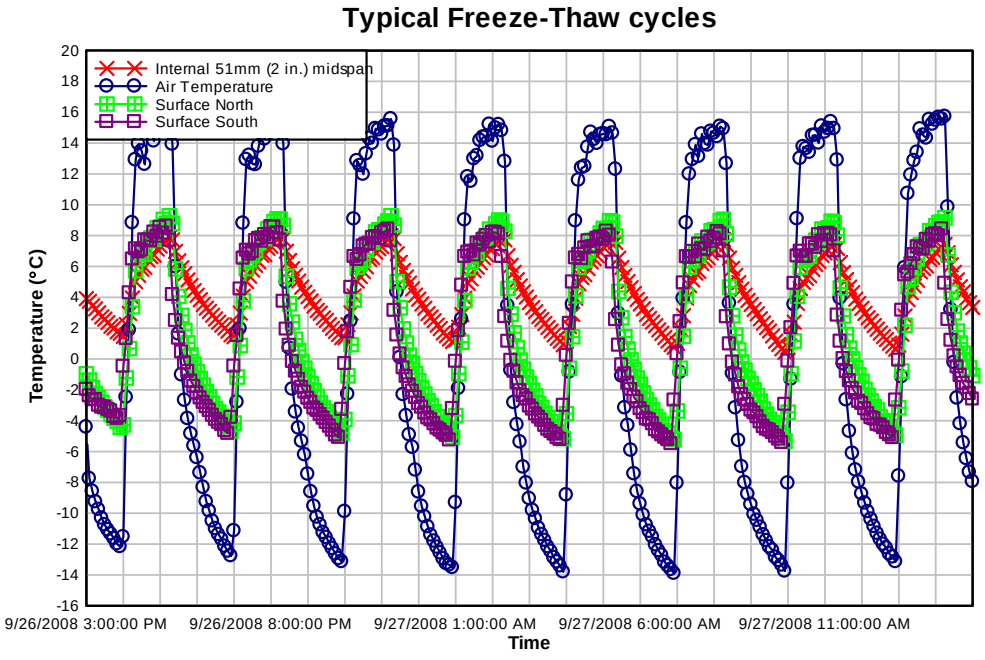

Fig. 4.12 – Typical temperature measurements during freeze-thaw cycling.

5 EXPERIMENTAL RESULTS

After installation of the CFRP and the environmental exposure, the specimens were moved to the strong floor and tested to failure. The experimental findings for each specimens and comparisons between measured responses are reported in this section. The salient structural response quantities for all specimens are contained in Table 5.1.

Table 5.1: Structural response quantities.

Specimen	V_{app} (kN) [kip]	V_{DL} (kN) [kip]	Midspan Displacement (mm) [in]
IT12Control	1179 [265]	22 [5]	30 [1.19]
T18Control	988 [222]	22 [5]	30 [1.18]
IT12M	1134 [255]	22 [5]	34 [1.34]
IT12MCK	1074[241]	22[5]	26[1.04]
ITT12FTCK	1136 [255]	22[5]	25 [1.01]
T18FFTCK	1005 [226]	36 [8]	28 [1.11]

5.1 Specimen IT12Control

Specimen IT12Control was initially tested using the increasing amplitude cyclical loading protocol. After achieving the maximum load in each cycle, visual inspection was performed to track cracks at the concrete surface and debonding of the CFRP. Debonding of the CFRP was identified by tapping the CFRP surface and listening for a distinct hollow sound. The specimen was loaded to 2224 kN (500 kips) which corresponded to the nominal capacity of the hydraulic actuator but the specimen did not fail. To produce a shear dominated failure, every other CFRP strip was removed and the load reapplied with the hydraulic system pressure increased to permit failure of the specimen. The applied shear at failure was 1179 kN (265 kips) with a midspan displacement of 27 mm (1.06 in.). The failure crack angle was approximately 30° from horizontal and crossed the three CFRP U-wraps closest to midspan as shown in Fig.5.25. The applied shear-midspan

displacement response of the specimen is shown in Fig 5.5 and the concrete cracking and CFRP debonding at the load step prior to failure are shown in Fig 5.24.

5.2 Specimen T18Control

Specimen T18Control was loaded in the same manner as the IT specimens to a load of 1975 kN (444 kips). Failure occurred at an applied shear of 988 kN (222 kip) with a midspan displacement of 30.0 mm (1.18 in.). The failure crack angle was approximately 30° degrees from horizontal, crossing the 2nd, 3rd and 4th CFRP U-wraps away from midspan. Shear and midspan displacements for each load cycle are shown in Fig. 5.5, while crack and debonding condition at the load step prior to failure is shown in Fig 5.24.

5.3 Specimen IT12M

Specimen IT12M was tested in a similar manner to IT12Control up to a load of 2224 kN (500 kips) and produced a midspan displacement of 23 mm (0.9 in.). After the initial load step, the capacity of the actuator was increased and the 2393 kN (538 kip) load step was repeated resulting in a midspan displacement of 27 mm (1.06 in.) on the second cycle, without failure. The specimen was again loaded with a maximum load of 2464 kN (554 kip) and the load deflection curve turned flat with midspan deflection 31 mm (1.24 in), flexural failure was imminent. As shear failure was not achieved, every other CFRP strip was removed, but in this case only first two alternate strips were removed and the 2224kN (500 kips) load was applied producing 32mm (1.27 in). The final failure diagonal crack passed through two CFRP sheets but the fourth strip (the one which should be have been removed) was able to maintain the beam strength, even as the crack crossed near the edge

of the strip. Before going on to the next load step, the fourth CFRP strip was removed and the beam failed at a shear of 1134 kN (255 kips) with midspan displacement 34 mm (1.34 in). The failure crack was similar to Specimen IT12Control, as the angle was approximately 30° degrees from horizontal and crossed the three CFRP U-wraps nearest midspan. Load deformation response and crack and debonding conditions at the load step prior to failure are shown in Fig. 5.5, Fig 5.7 and Fig. 5.24 at the end of chapter.

5.4 Specimen IT12MCK

Specimen IT12MCK was also tested using increasing amplitude cyclical loading to 2224 kN (500 kips). It was loaded to 2375 kN (534 kips) after increasing the actuator capacity. After removing alternate CFRP strips, failure occurred at 2144 kN (482 kips) load with midspan displacement 26mm (1.04 in). Load deformation response, crack and debonding conditions at the load step prior to failure are shown in Fig.5.5, Fig.5.8 and Fig. 5.24, respectively. The failure crack, shown in Fig 5.25, was similar to the other IT specimens, crossing the three CFRP U-wraps nearest load application with an angle of approximately 30° from horizontal.

5.5 Specimen ITT12FTCK

Specimen ITT12FTCK was tested in a similar way for the first load cycle step to 2224 kN (500 kips). As per the previous tests, for shear dominant failure, alternate strips were removed and again the load step of 2224 kN (500 kips) was repeated. It was then loaded with increased actuator capacity to 2268 kN (510 kips), failing with an ultimate midspan displacement of 26 mm (1.01 in). Load deformation response and crack and debonding conditions at the load step prior to failure are shown in Fig.5.5, Fig.5.9 and Fig. 5.24,

respectively. The failure crack, shown in Fig 5.25, was similar to the other IT specimens, crossing the three CFRP U-wraps nearest load application with an angle of approximately 30° from horizontal.

5.6 Specimen T18FFTCK

Specimen T18FFTCK was loaded cyclically to 2019 kN (454 kips). Failure occurred at an applied shear of 1010 kN (227 kip) with a midspan displacement of 28 mm (1.11 in.). The failure crack angle was approximately 30° from horizontal, crossing the 3rd, 4th, and 5th CFRP U-wraps away from midspan. This specimen seems contained less moisture as compared to the freeze-thaw T- specimens tested previously (Mikal 2008). Load deformation response and crack and debonding conditions at the load step prior to failure are shown in Fig.5.5, Fig.5.10 and Fig. 5.24, respectively.

5.7 Comparison of Pre-Strengthening – Post-Strengthening Responses

The changes in structural response of the specimens provided by the CFRP strengthening and the role of environmental durability is of particular interest to this study. A key issue is the additional shear strength provided by the CFRP. Because the CFRP strengthened specimens contained different concrete material properties, it becomes necessary to estimate the base capacity of the specimens without the addition of CFRP. Previous research on unstrengthened RC girders of the same proportions and similar materials were conducted at Oregon State University [Higgins *et al*. 2004]. The reported shear capacities of identical IT and T configurations with similar shear and flexural steel reinforcing ratios to those tested here were, 921 kN (207 kips) and 756 (170 kips) respectively. Importantly, the strength of a large suite of similar beams with different shear and flexural details were

predicted with a program called Response-2000 (R2K). This program was developed at the University of Toronto [Bentz 2001] and uses a nonlinear sectional analysis based on MCFT to predict shear-moment capacity of RC elements. Application of this program to a suite of 44 similar full-scale RC specimens tested at Oregon State University predicted the unrepaired member capacity to within 2% with a coefficient of variation under 8% [Higgins *et al*. 2004]. In order to compare base specimen capacity to CFRP strengthened capacity, R2K was used. Results of R2K for the conventional RC girders without CFRP are shown with the present CFRP strengthened T and IT specimens in Fig. 5.1 and numerical results are reported in Table 5.2 where V_{EXP} is the sum of the applied shear, V_{app}, and the specimen self-weight acting at the failure crack, V_{DL}, and V_{R2k_B} is the unstrengthened base specimen shear capacity predicted by Response-2000. In Fig. 5.2, the results are normalized with respect to the concrete and shear reinforcing properties.

The effect of adding CFRP on stiffness was also of interest. Comparisons of responses without environmental exposure can be made using Specimens IT12Control, IT12M, IT12MCK, ITT12FTCK, T18Control, and T18FFTCK, considering both the overall member stiffness as indicated by the midspan displacement and individual shear panel stiffness measured within the six different diagonally instrumented shear panels. Changes were observed by comparing the precrack baseline response (pre-strengthening) to the recrack response (post-strengthening) for the Ck specimens, and comparing the precrack baseline response (pre-strengthening) to the failure response (post-strengthening) for the control specimens. The overall specimen stiffnesses can be examined in Fig 5.12.

Table 5.2: Measured shear capacity for strengthened and predicted shear strength of base specimens (specimen without CFRP).

Specimen	V_{EXP} (kN) [kip]	V_{R2k_B} (kN) [kip]
IT12Control	1201 [270]	912 [205]
T18Control	1010 [227]	752 [169]
IT12M	1134 [255]	943 [212]
IT12MCK	1074[241]	921 [207]
ITT12FTCK	1136 [255]	907 [204]
T18FFTCK	1005 [226]	769 [173]

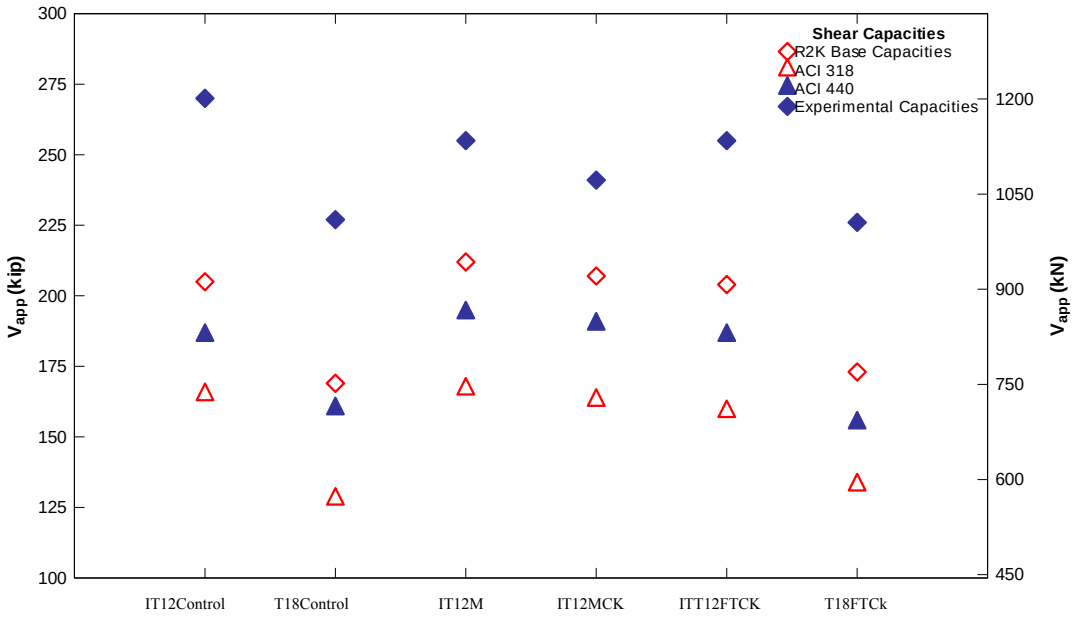

Fig. 5.1 – Shear capacities for all specimens.

Stiffness changes were not apparent in any of the specimens when considering midspan displacements. This is reasonable, as midspan displacements are dominated by flexural deformations and increasing shear reinforcement has little effect on flexural deformations. Shear in panel are compared in curves given from Fig. 5.13 to Fig. 5.23.

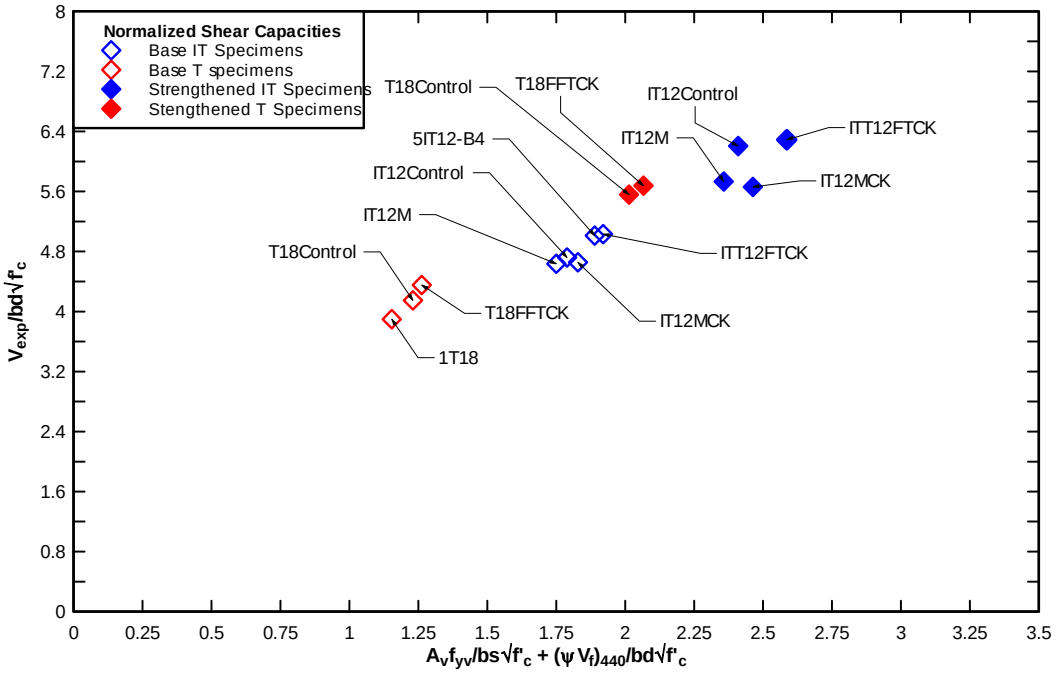

Fig. 5.2 – Normalized shear capacities for all specimens.

A slight change in stiffness due to CFRP application was seen across all specimens. Shear panel 3 is located nearest midspan where diagonal cracking is not apparent until higher loads. As the panel is typically already stiff at lower load, an increase in stiffness is more difficult to detect. Finally, shear panel 2 stiffnesses can be compared using Fig. 5.13 to Fig. 5.23. The change in stiffness due to CFRP application was very apparent in shear panel 2. This panel is located in the middle of the shear span and typically exhibits significant diagonal cracking through the height of the web. The increased shear reinforcement provided by the CFRP constrained the crack deformations well. It is also likely the smearing effect of the CFRP strips provide better crack control than discrete internal steel stirrups.

5.8 Comparison of Pre-Exposure – Post-Exposure Responses

In order to identify environmental effects on the specimens, changes in stiffness were considered. Both overall specimen stiffness (applied shear vs. midspan displacement) and individual panel stiffnesses (applied shear vs. average vertical strain) were investigated. Specimen IT12MCK, ITT12FTCK, and Specimen T18FTCk were recracked after strengthening. After recracking, these specimens were cyclically reloaded to produce a baseline for post-exposure comparison. Any change in stiffness post-exposure can be attributed to the effects of the environmental exposure. Changes were observed by comparing the recrack baseline response (pre-exposure) to the failure response (post-exposure). The overall specimen stiffnesses for all specimens are compared are shown in Fig.5.6, Fig5.11 and Fig. 5.12. A change in stiffness due to exposure was not apparent in either specimen when the midspan displacements were examined. Again this is reasonable as additional shear reinforcing did not appear to increase the overall stiffness and thus any degradation of the shear reinforcing due to environmental exposure would not significantly impact the overall stiffness.

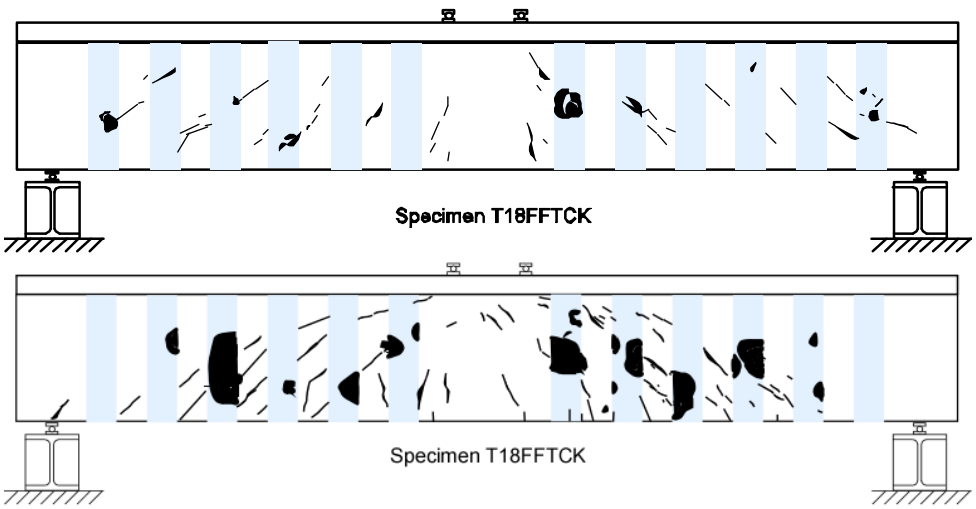

Fig. 5.3 – Cracked and debonded condition of Specimen T18FTCk pre-exposure and post-exposure.

5.9 Internal Strain Gage Data

Data were collected from internal stirrup strain gages. While local strain data can be useful, it did not provide insight into freeze-thaw effects. Strain gage results depend heavily on their location relative to the diagonal cracks. Due to varying crack patterns, local strain data were difficult to compare across specimens. Additionally, these internal strain gages were often damaged during casting, precracking or recracking. Due to the CFRP application, chipping into the concrete and repairing the strain gages was not possible.

5.11 Specimen Orientation

As seen in the results discussed above, freeze-thaw exposure did not appear to adversely affect the additional shear response or strength gained for CFRP strengthening of the IT specimens where no significant moisture was apparent in the interface between the concrete and CFRP, while it significantly affected the capacity of the T specimens where such moisture was apparent in the bonding interface. Moisture appears to play a significant role in the effect of freeze-thaw exposure. The difference in moisture seen in the specimens may be attributed to the orientation of the specimens during CFRP application and freeze-thaw exposure whereby water can get into the interface from the free edge and be trapped behind the CFRP composite layer and repeated expansion and contraction leads to bond deterioration. The terminating edges of the CFRP strips being of particular interest.

During CFRP application on the IT specimens, the fibers were impregnated by running the putty knife downward toward the free edge of the strip near the flange. This allowed

excess saturant to puddle at the free edge of the CFRP strips at the flange interface. During CFRP application on the T specimens, the fibers were impregnated by running the putty knife upward toward the free edge of the strip near the flange. Gravity did not allow saturant to puddle along the free edge in this case. This added epoxy matrix at the strip edge and deck-step interface appears to have limited the ability of moisture to enter the CFRP-concrete interface and at the strip termination. During freeze-thaw exposure the specimens were oriented in the same manner as during testing. For the T specimens this meant there was exposed concrete on the top of the beam, where moisture could enter the specimen, but a moisture barrier at the bottom of the specimen. If moisture was continually working downward through the girder, this allowed for ingress but no egress. The opposite was true for the IT specimens. The CFRP formed a moisture barrier at the top of the specimen while concrete was exposed at the bottom. In order for moisture to enter the web, it would have to wick upward or through available cracks.

5.12 Thermally Induced Strains

Concrete and CFRP have very different coefficients of thermal expansion (CTE) causing thermally induced strains at the bond interface during freeze-thaw. Normal-weight concrete has a CTE ranging from 9-12.6 x 10^{-6} /°C (5-7 x 10^{-6} /°F) [MacGregor and Wight 2005], while Wabo® reports a CTE of -0.38 x10^{-6} /°C (-0.21 x10^{-6} /°F) for the CFRP. Not only are the CTEs orders of magnitude different, they have opposite signs indicating one expands while the other contracts and vice versa. As seen in Fig. 4.12, the surface of the specimens experienced a temperature range of 20°C (36°F) during freeze-thaw exposure, resulting in a strain range of 188 -260 με. However, the surface strain data shown in Fig.5.4 does not match well with the above strain range.

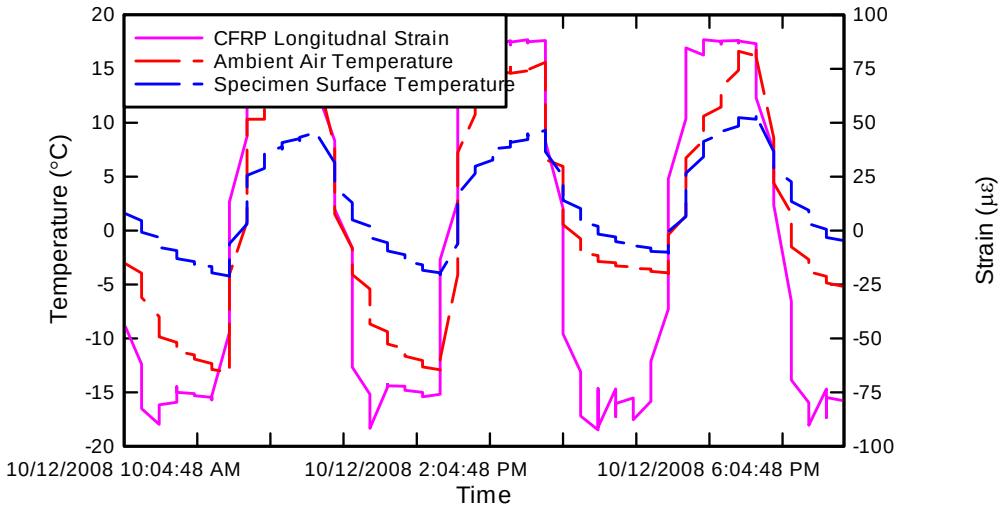

Fig. 5.4 – Freeze-thaw cycling and associated CFRP surface strains.

Thermally induced strains of this magnitude up to 550 cycles do not appear to have a detrimental effect, as no loss in shear capacity was seen for the IT specimens. In the field, bridge members may undergo even larger surface temperature fluctuations daily. No conclusions can be drawn from this data about the long-term effect of larger thermally induced strains in the field.

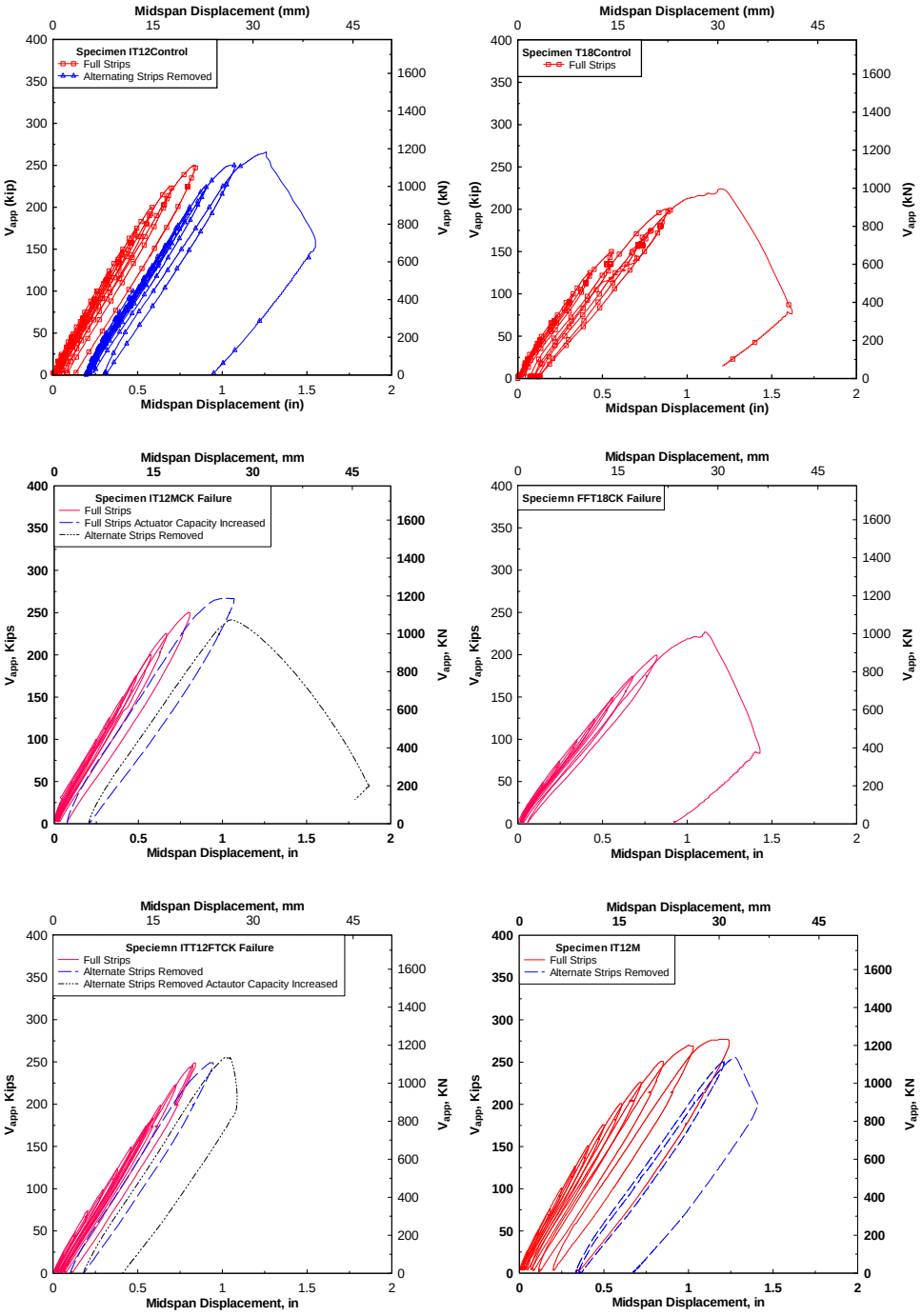

Fig 5.5 - Midspan Shear – Deflection curves at Failure compared with control specimen

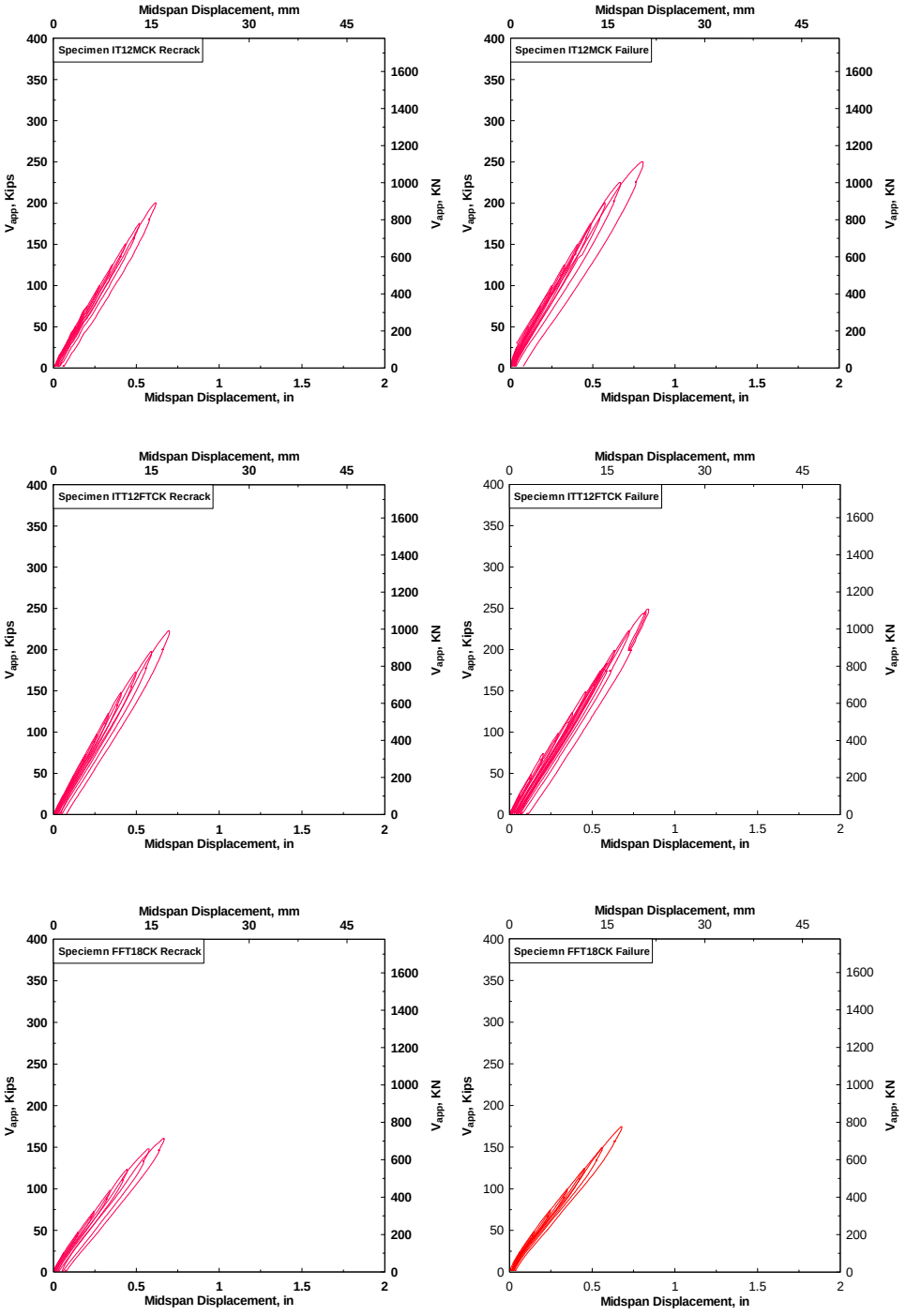

Fig 5.6 - Pre and Post Environmental Midspan Shear Deflection curves

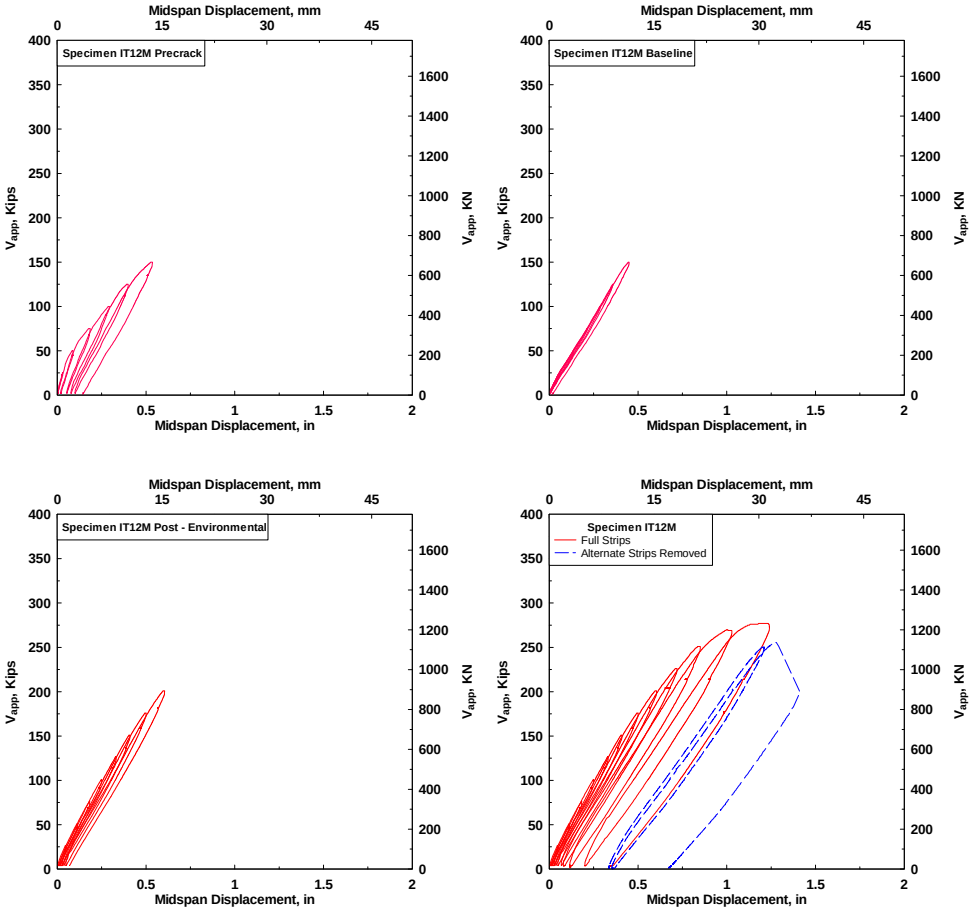

Fig 5.7 - Specimen IT12M Midspan Shear Deflection curves

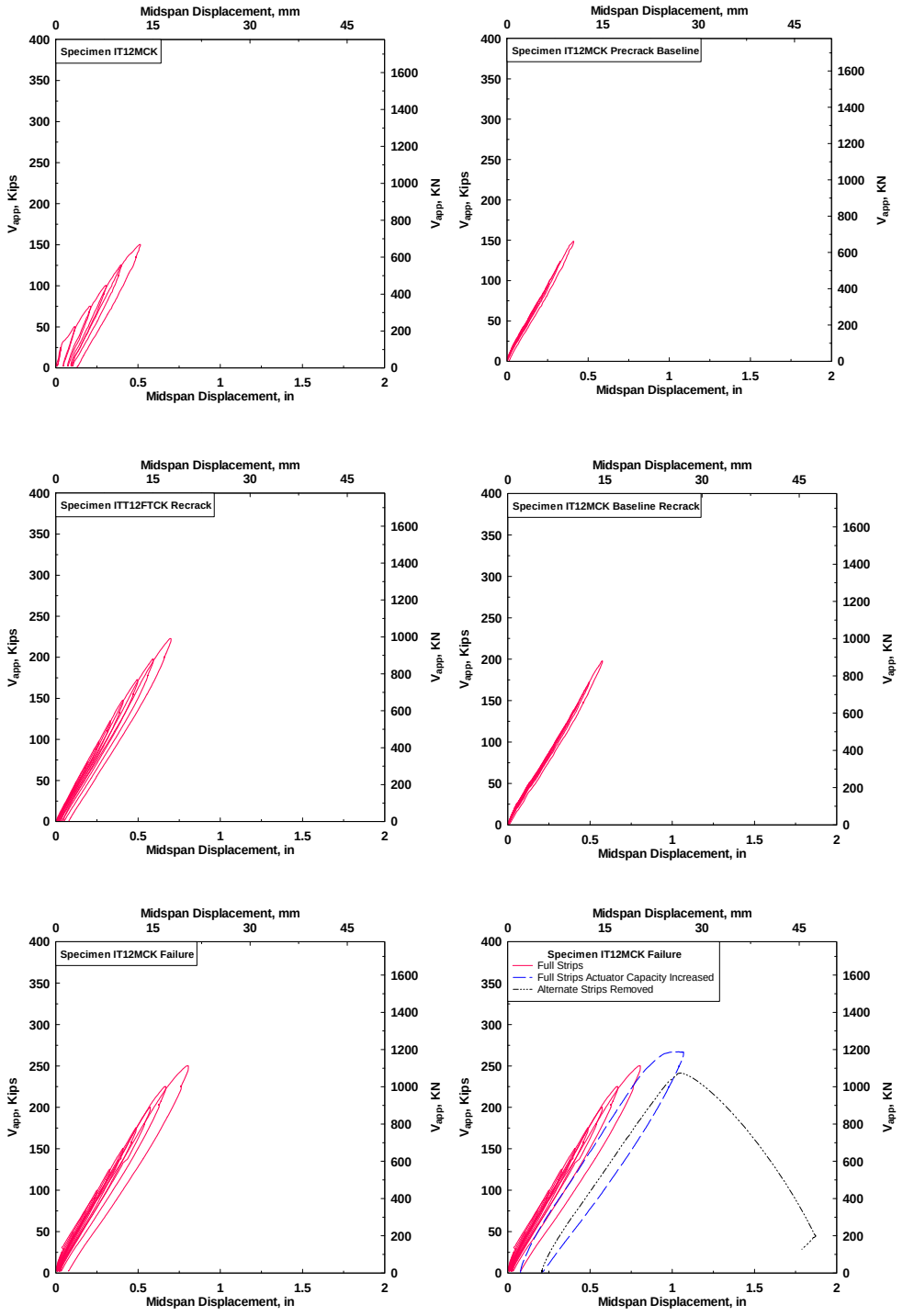

Fig 5.8 - Specimen IT12MCK Midspan Shear Deflection curves

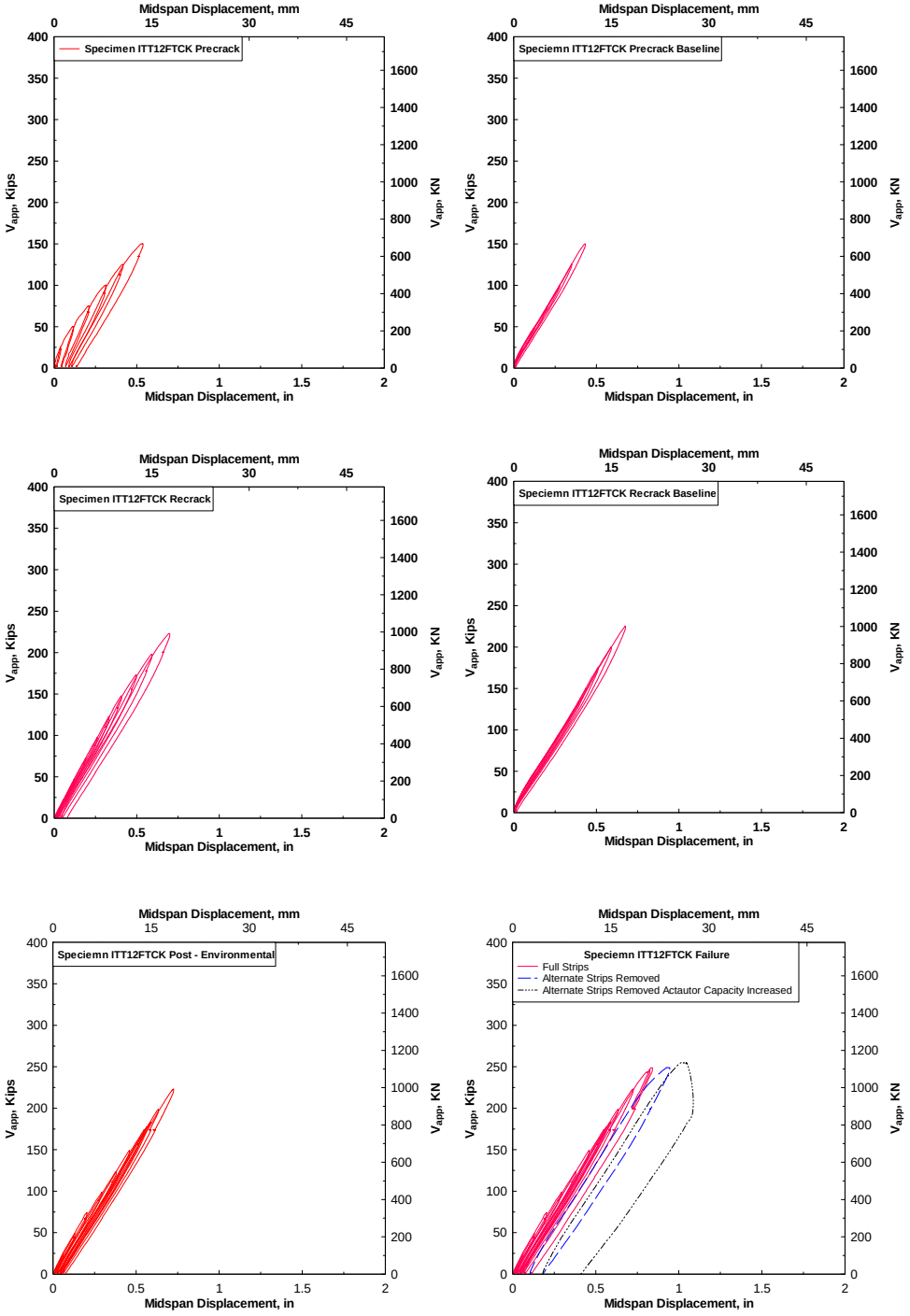

Fig 5.9 - Specimen ITT12FTCK Midspan Shear – Deflection curves

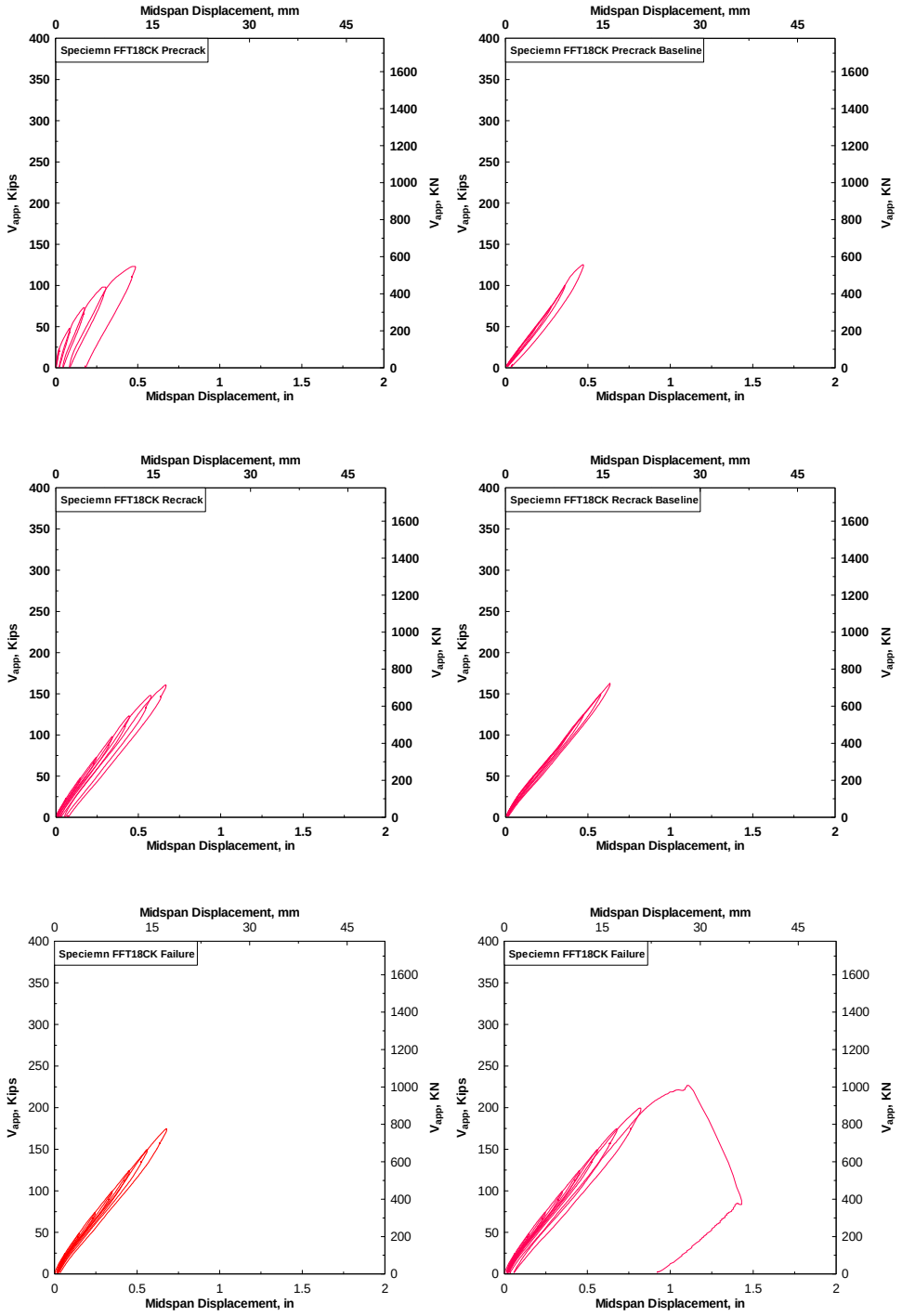

Fig 5.10 - Specimen T18FFTCK Midspan Shear Deflection curves

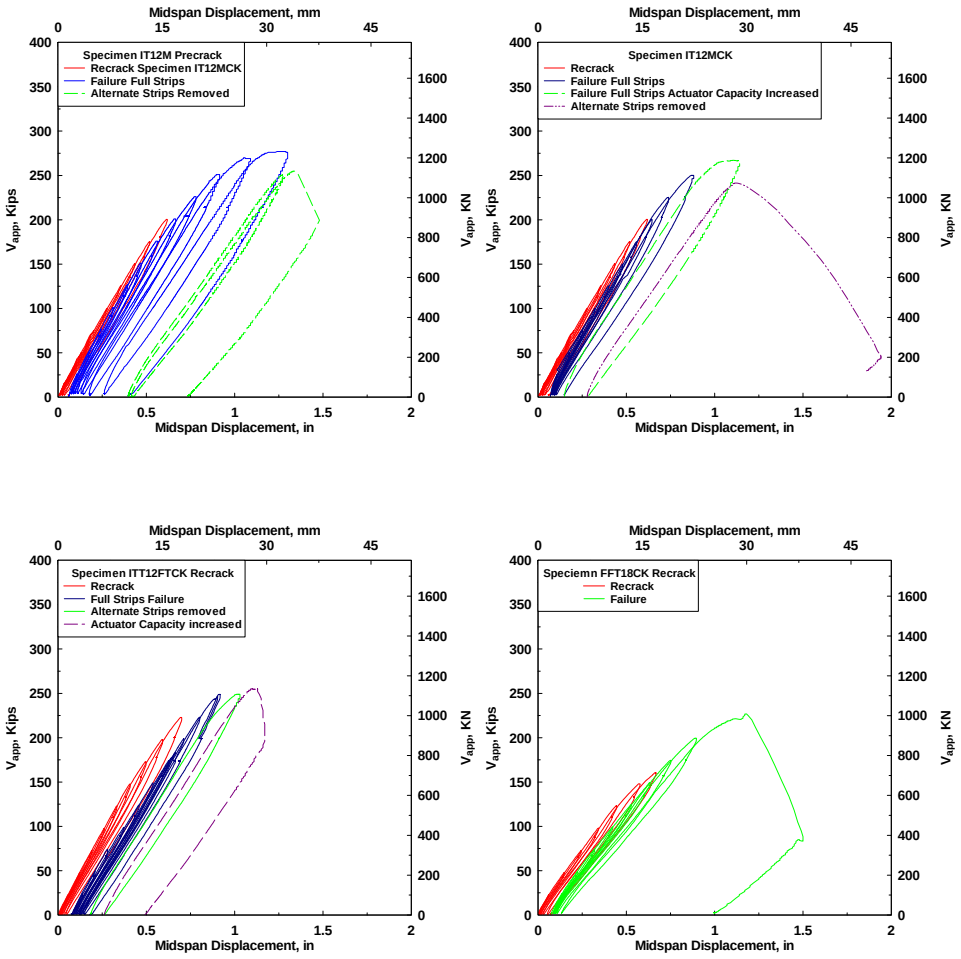

Fig 5.11 - Midspan Shear – Deflection curves Pre-Environmental and Failure comparison

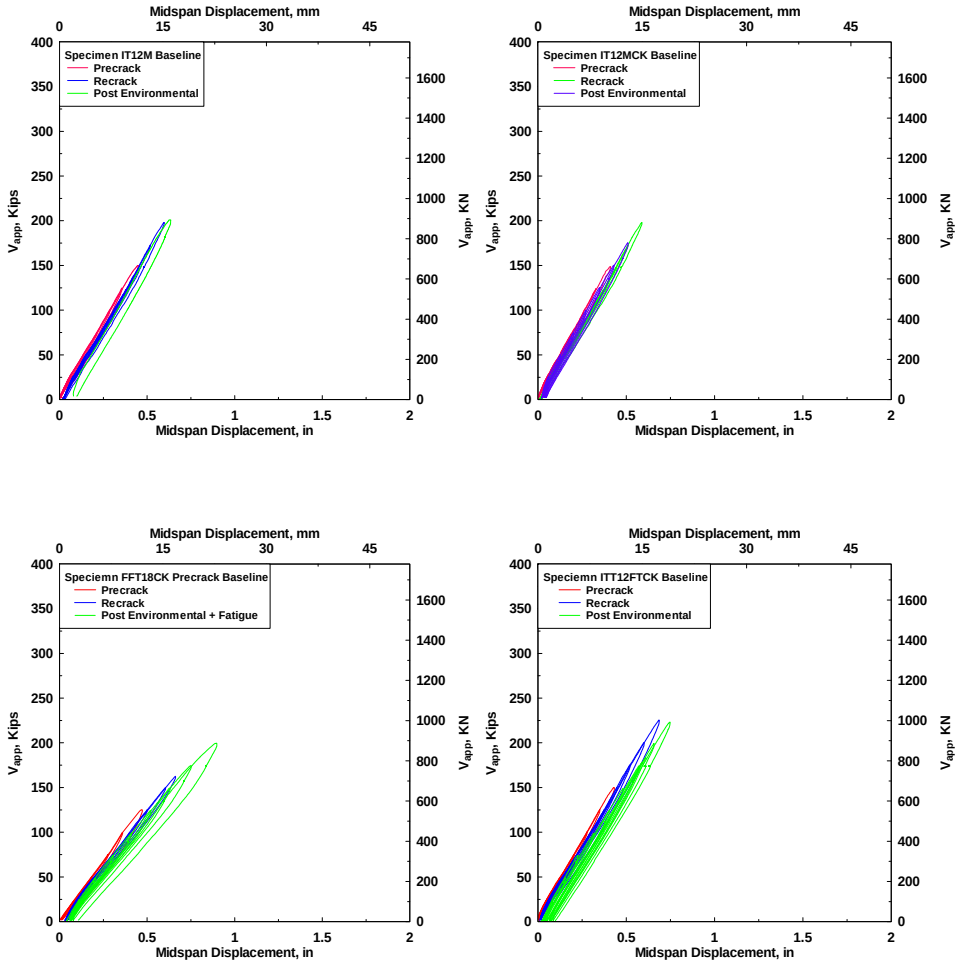

Fig 5.12 - Midspan Shear Deflection curves Stiffness comparison

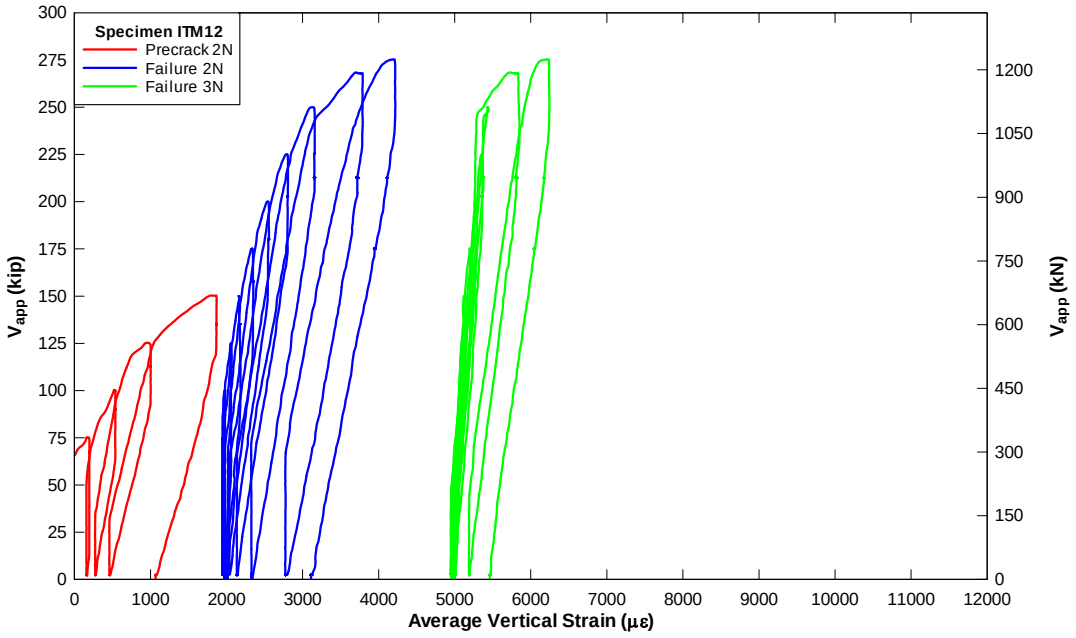

Fig 5.13 - Specimen IT12M – Shear Panel 2N

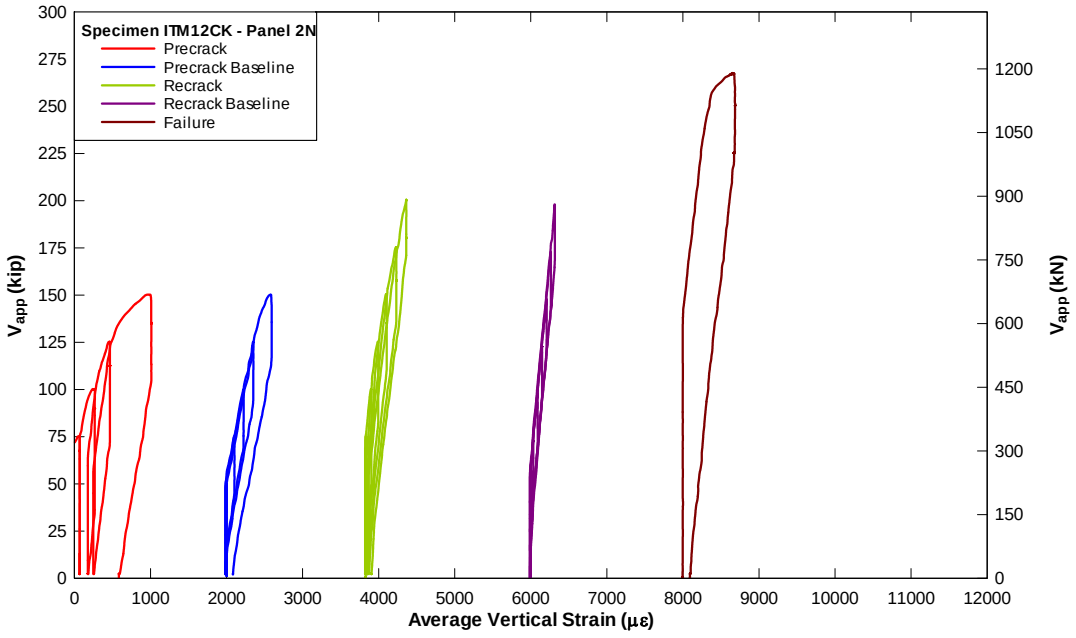

Fig 5.14 - Specimen IT12MCK – Shear Panel 2N

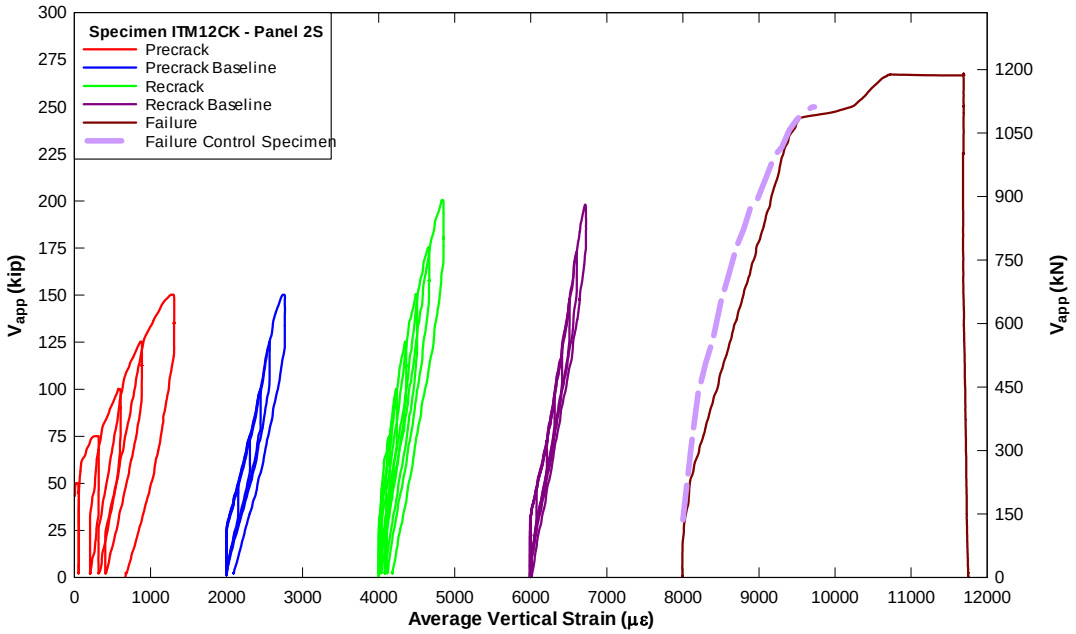

Fig 5.15 - Specimen IT12MCK – Shear Panel 2S

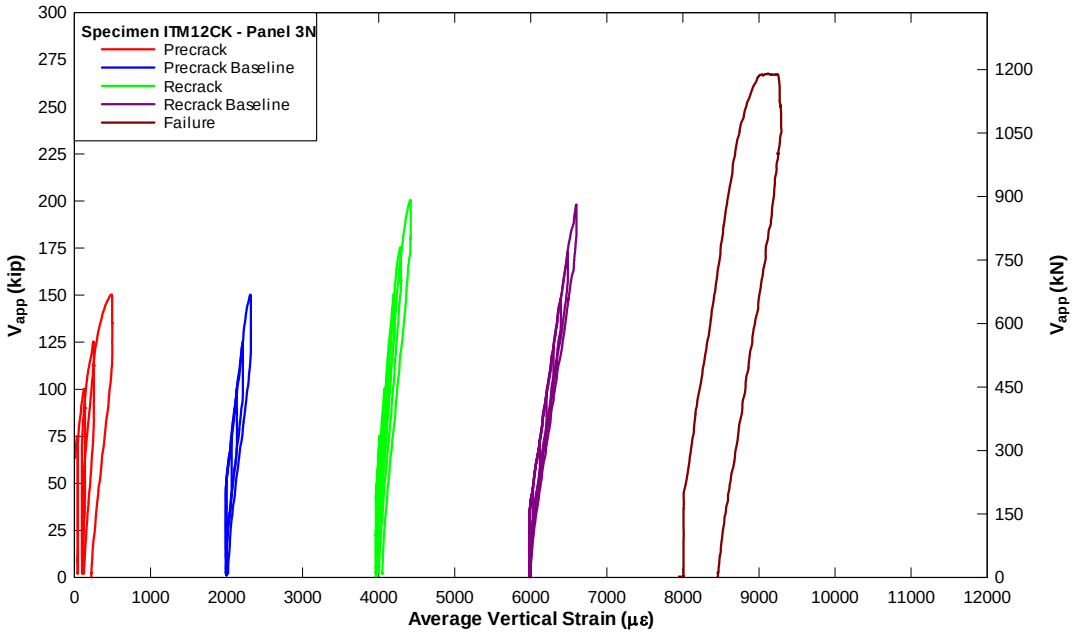

Fig 5.16 - Specimen IT12MCK – Shear Panel 3N

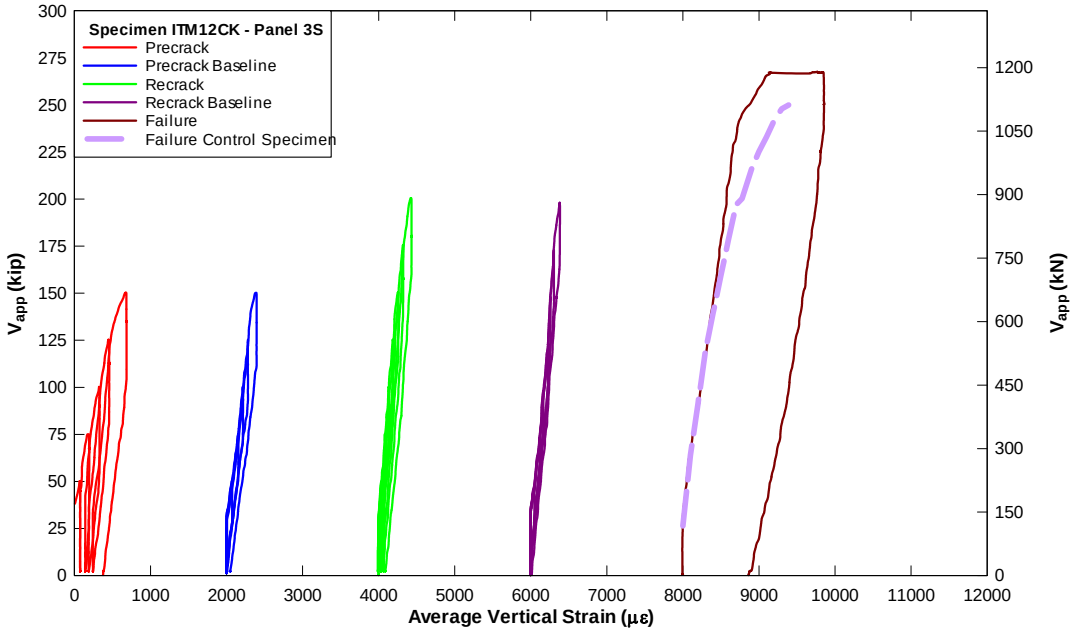

Fig 5.17 - Specimen IT12MCK – Shear Panel 3S

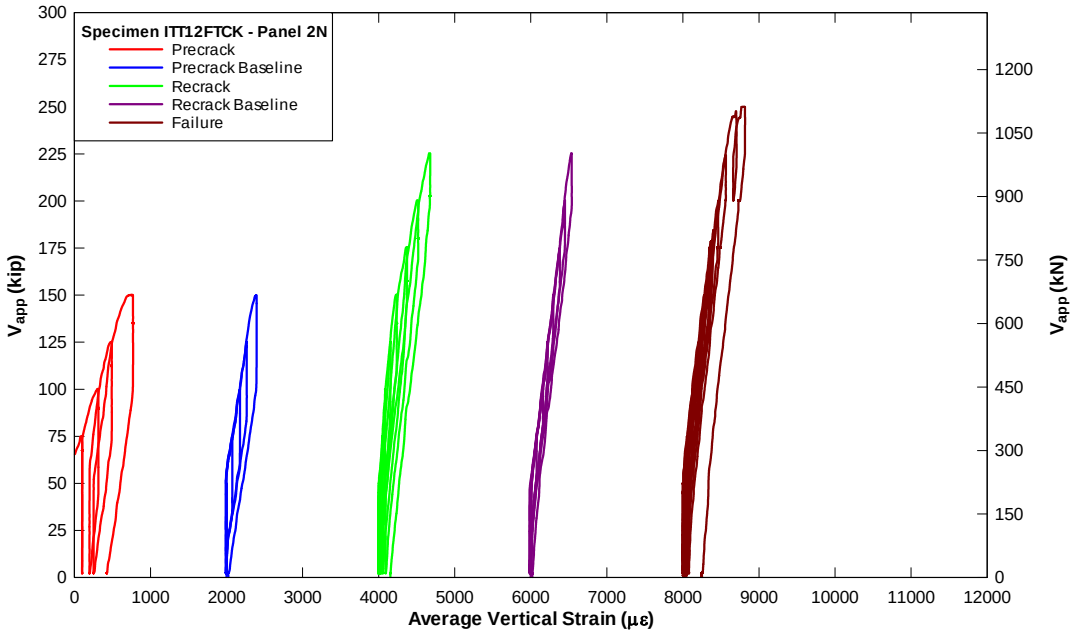

Fig 5.18 - Specimen ITT12FTCK – Shear Panel 2N

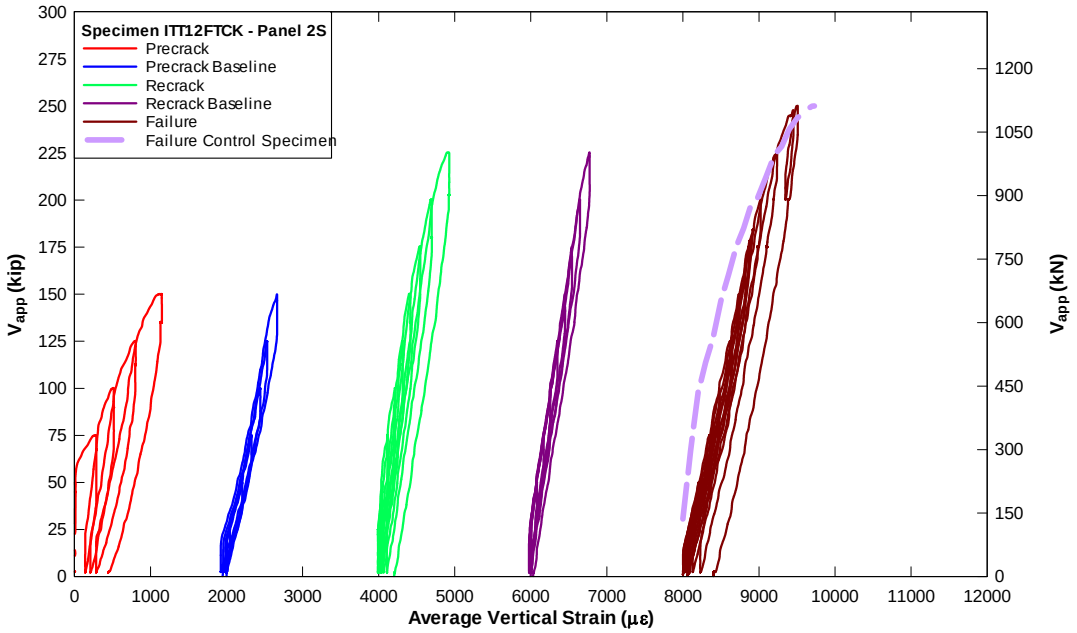

Fig 5.19 - Specimen ITT12FTCK – Shear Panel 2S

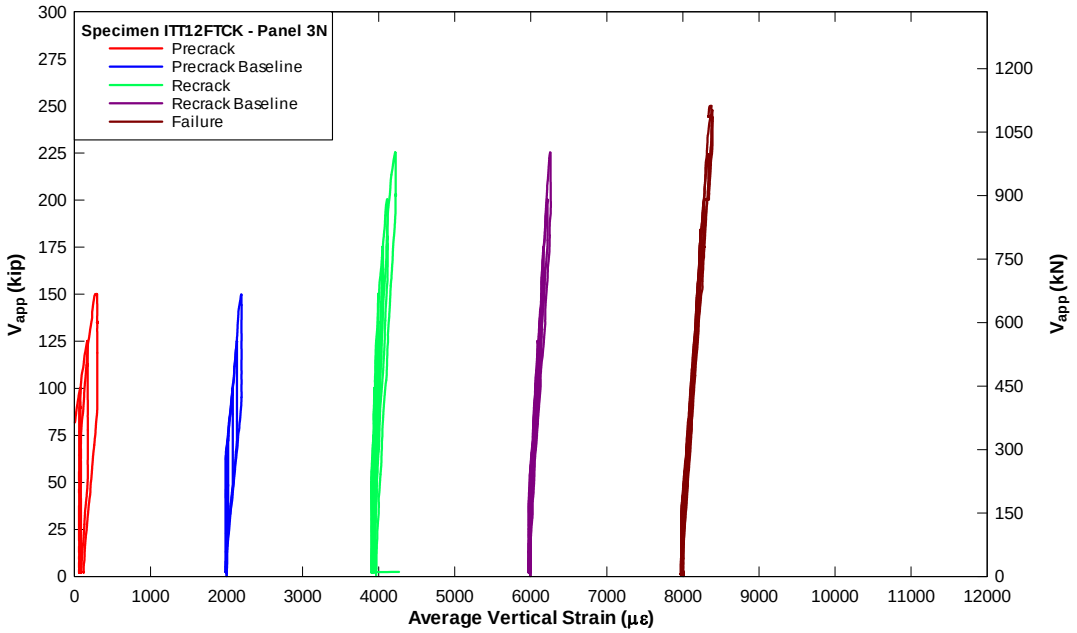

Fig 5.20 - Specimen ITT12FTCK – Shear Panel 3N

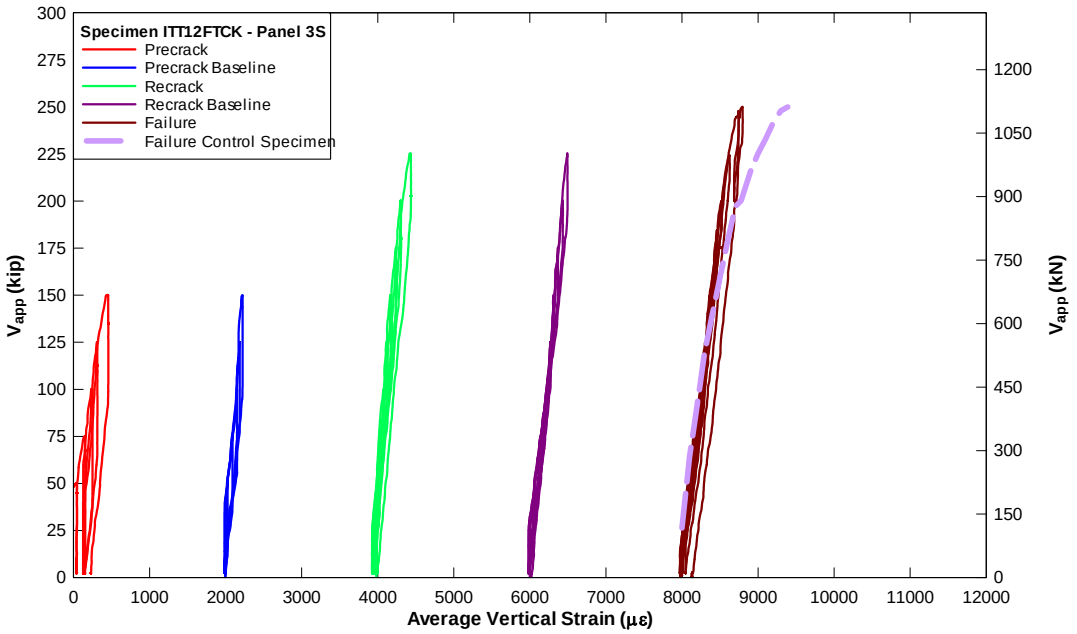

Fig 5.21 - Specimen ITT12FTCK – Shear Panel 3S

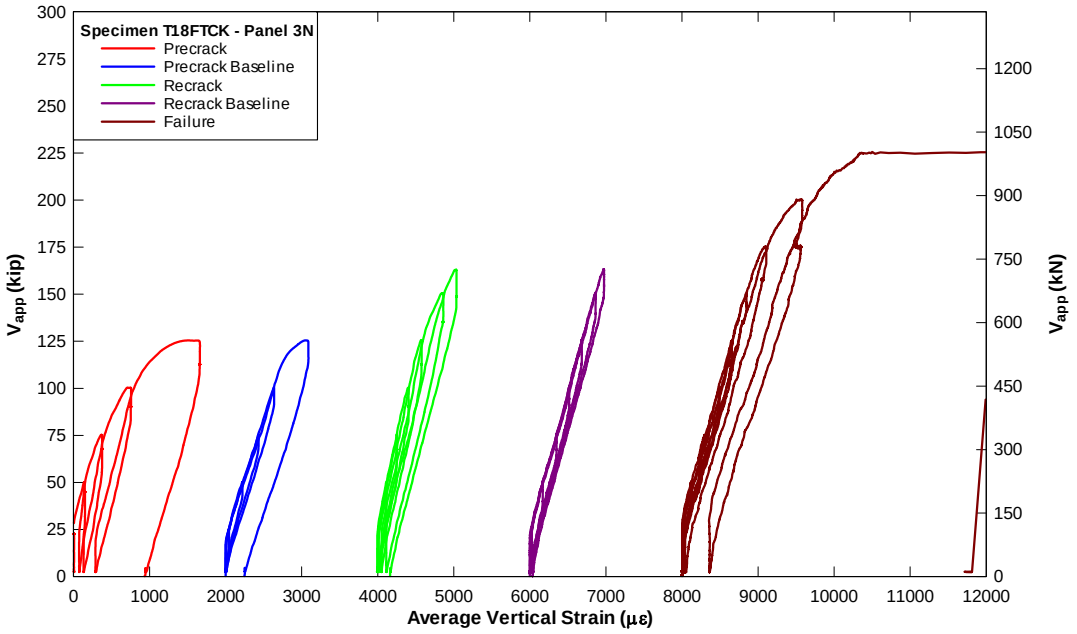

Fig 5.22 - Specimen T18FFTCK – Shear Panel 3N

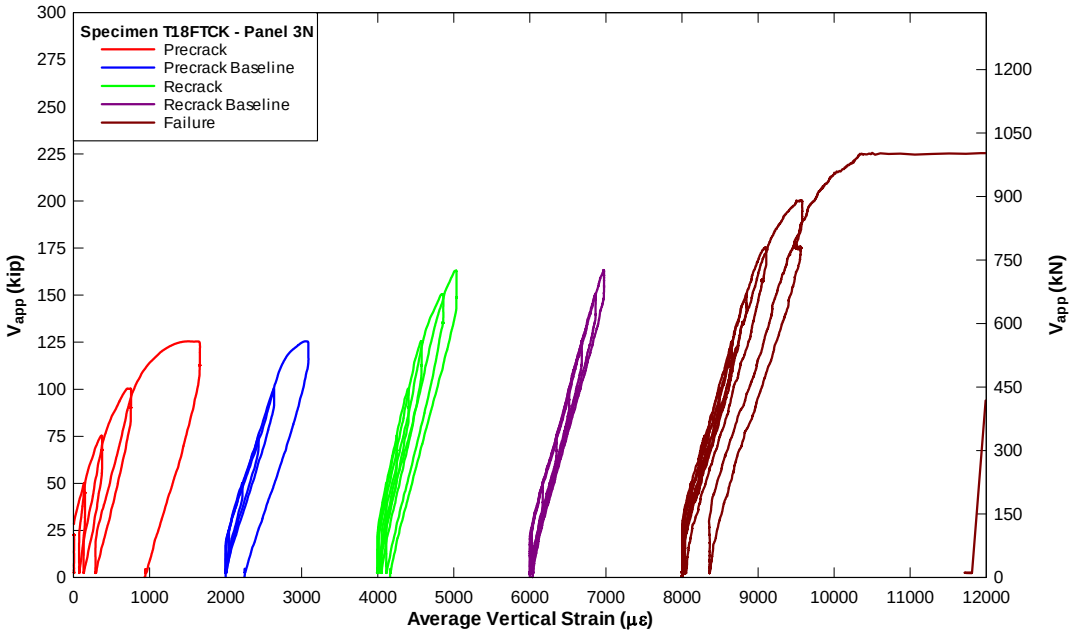

Fig 5.23 - Specimen T18FFTCK – Shear Panel 3N

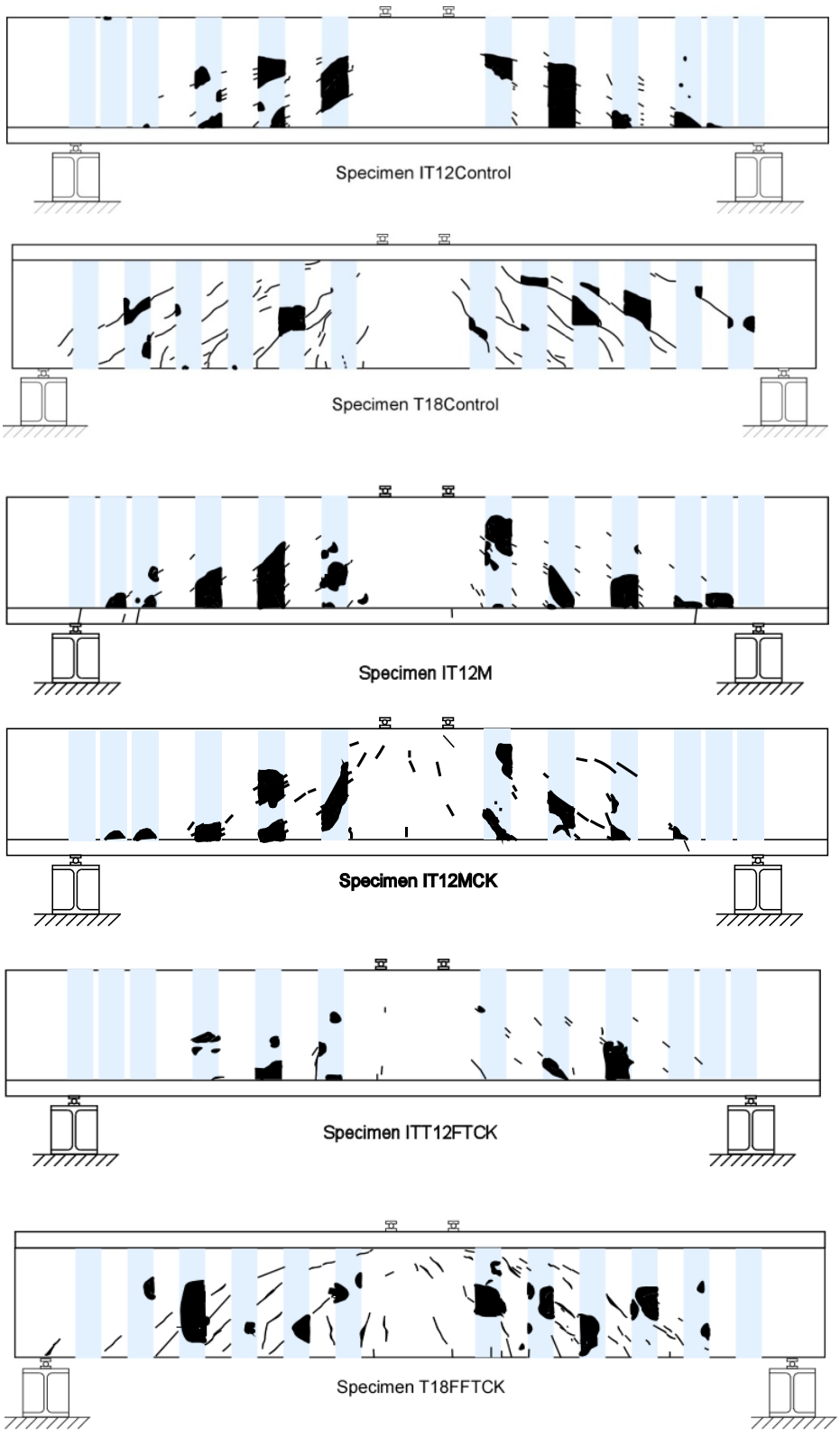

Fig 5.24 - Cracked and debonded condition at Failure

Fig 5.25 - Failure photographs for all specimens

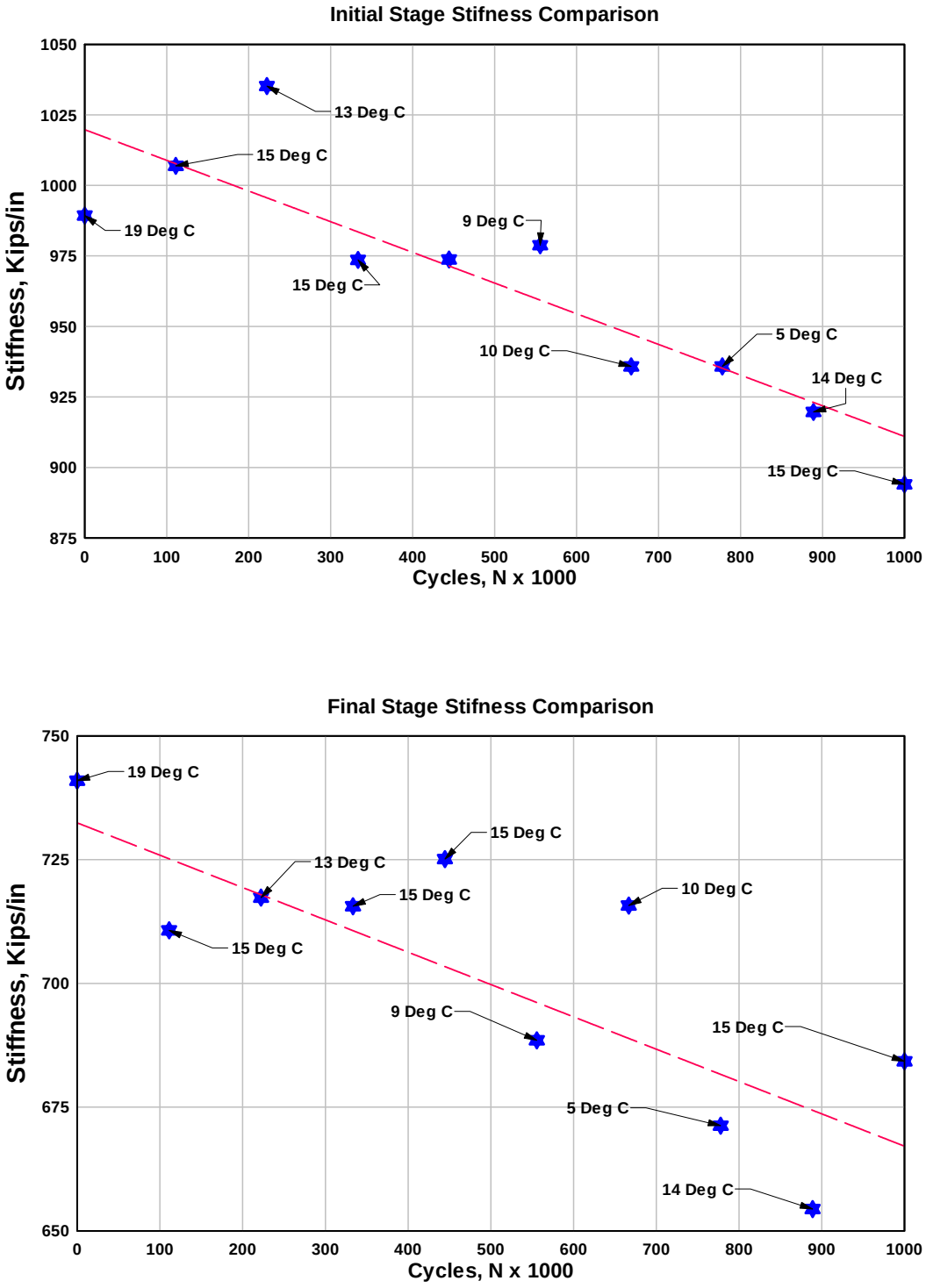

Fig 5.26 - Stiffness Comparison for Fatigue Specimen

6 COMPARATIVE ANALYSIS

The additional capacity provided by surface-bonded CFRP and the applicability of ACI-440.2R-02 to predict environmental performances are of particular interest for the current study. Unstrengthened control specimens were tested in a previous test series [Higgins *et al.* 2004] and the shear capacities were well predicted using the analysis program Response-2000. This same program was used to calculate the base capacities of the CFRP strengthened beams to account for variable material properties. Additionally, ACI 318-05 was used to calculate the base specimen capacities for comparison. Finally, ACI-440 was used to calculate the expected additional shear capacity provided by the CFRP. These analysis results are discussed in the following section.

6.1 Base Capacity Prediction

Response-2000 was used to predict the base capacities of the specimens. Actual day-of-test compressive concrete strengths along with actual flexural and transverse steel properties determined from material testing and reported in Table 4.1 were used in the analysis. The shear strength was predicted at the location d_v away from the edge of the loading plate (near midspan) and resulted in a M/V ratio of 1859 mm (73.2 in.) and 2225 mm (87.6 in.) for the IT and T specimens, respectively. The analysis results are shown in Table 6.1.

The base capacity of the specimens was also calculated according to ACI 318-05 by superimposing the concrete shear contribution, V_c (N) [lb], and the transverse steel shear contribution, V_s (N) [lb] as:

$$V_n = V_c + V_s \qquad \text{(11-2) US} \quad [6.1]$$

The concrete contribution was computed as:

$$V_c = 2\sqrt{f_c'}b_w d \qquad \text{(11-3) US} \quad [6.2]$$

where f_c' = concrete compression strength (MPa) [psi], b_w = beam width (mm) [in.], d = effective depth (mm) [in.]. The steel contribution was calculated as:

$$V_s = \frac{A_v f_{yt} d}{s} \qquad \text{(11-15) US} \quad [6.3]$$

where A_v = area of transverse steel reinforcement (mm^2) [$in.^2$], f_{yt} = transverse steel yield strength (MPa) [ksi] and s = spacing (mm) [in.]. Again, actual day-of-test compressive concrete strengths and the actual steel properties were used in this analysis and results are shown in Table 6.1.

6.2 CFRP Shear Contribution from ACI 440.2R-02

The surface-bonded CFRP contribution to shear capacity was determined using ACI 440.2R-02 which adds a FRP shear contribution term, V_f (N) [lb], to the base specimen capacity determined using ACI 318-05 from Eqn. 6.1. The FRP shear contribution term is determined as:

$$V_f = \frac{A_{fv} f_{fe} (\sin\alpha + \cos\alpha) d_f}{s_f} \qquad \text{(10-3)} \quad [6.4]$$

where α (°) is the FRP strip orientation from the horizontal axis, d_f (mm) [in.] is the depth of FRP reinforcement, s_f (mm) [in.] is the FRP strip spacing, f_{fe} (MPa) [ksi] is the effective FRP strength, and A_{fv} (mm^2) [$in.^2$] is the area of FRP shear reinforcement. A_{fv} is calculated using the FRP strip width, w_f (mm) [in.], number of layers, n, and FRP thickness, t_f (mm) [in.] as:

$$A_{fv} = 2nt_f w_f \qquad \text{(10-4)} \quad [6.5]$$

The effective FRP strength, f_{fe}, is calculated using the FRP effective strain, ε_{fe}, and FRP elastic modulus, E_f (GPa) [ksi] as:

$$f_{fe} = \varepsilon_{fe} E_f \qquad \text{(10-5)} \quad [6.6]$$

The ultimate strain of the FRP, ε_{fu}, is limited to an effective strain, ε_{fe}, using the bond-reduction coefficient, κ_v, based on the active bond length, L_e (mm) [in.], and other FRP properties including, n, the number of FRP layers, t_f, the FRP thickness (mm) [in.], and E_f, the FRP elastic modulus (GPa) [ksi] as:

$$L_e = \frac{416}{(n\, t_f E_f)^{0.58}} \qquad \text{(10-7) SI} \quad [6.7]$$

$$L_e = \frac{2500}{(n\, t_f E_f)^{0.58}} \qquad \text{(10-7) US} \quad [6.8]$$

$$k_1 = \left(\frac{f_c'}{254} \right)^{2/3} \qquad \text{(10-8) SI} \quad [6.9]$$

$$k_1 = \left(\frac{f_c'}{4000} \right)^{2/3} \qquad \text{(10-8) US} \quad [6.10]$$

$$k_2 = \left(\frac{d_f - L_e}{d_f} \right) \qquad \text{(10-9)} \quad [6.11]$$

$$\kappa_v = \frac{k_1 k_2 L_e}{468 \varepsilon_{fu}} \le 0.75 \qquad \text{(10-10) US} \quad [6.12]$$

$$\varepsilon_{fe} = \kappa_v \varepsilon_{fu} \le 0.004 \qquad \text{(10-6b)} \quad [6.13]$$

where f_c' (MPa) [psi] is the concrete compression strength. The FRP shear contribution, V_f (N) [lb], is reduced using an additional factor, ψ_f, to account for the wrapping scheme and is taken as 0.85 for U-wrapping. The design shear strength is taken by superimposing the concrete, steel, and FRP contributions and applying the shear strength reduction factor of 0.85.

$$\phi V_n = \phi\left(V_c + V_s + \psi_f V_f\right) \qquad \text{(10-2)} \quad [6.14]$$

ACI-440 limits on the total amount of shear reinforcing (steel and FRP) as:

$$V_s + V_f \le 0.66\sqrt{f_c'}\,b_w d \qquad \text{(10-11)SI} \quad [6.15]$$

$$V_s + V_f \le 8\sqrt{f_c'}\,b_w d \qquad \text{(10-11)US} \quad [6.16]$$

to prevent web crushing.

6.3 Specimen Capacity Comparison

The strengthened specimen shear capacity found by taking the applied shear from the actuator, V_{app} (kN) [kip], and adding the specimen self-weight, V_{DL} (kN) [kip], acting at the failure diagonal crack to determine the experimental shear strength, V_{EXP} (kN) [kip]. This value was compared to the calculated base capacity using Response 2000, V_{R2k_B} (kN) [kip], the calculated base capacity using ACI-318 from Eqn. 6.1, V_{318} (kN) [kip], and the calculated strengthened specimen capacity using ACI-440 from Eqn. 6.14, V_{440} (kN) [kip] as illustrated in Fig. 6.1 and Table 6.1.

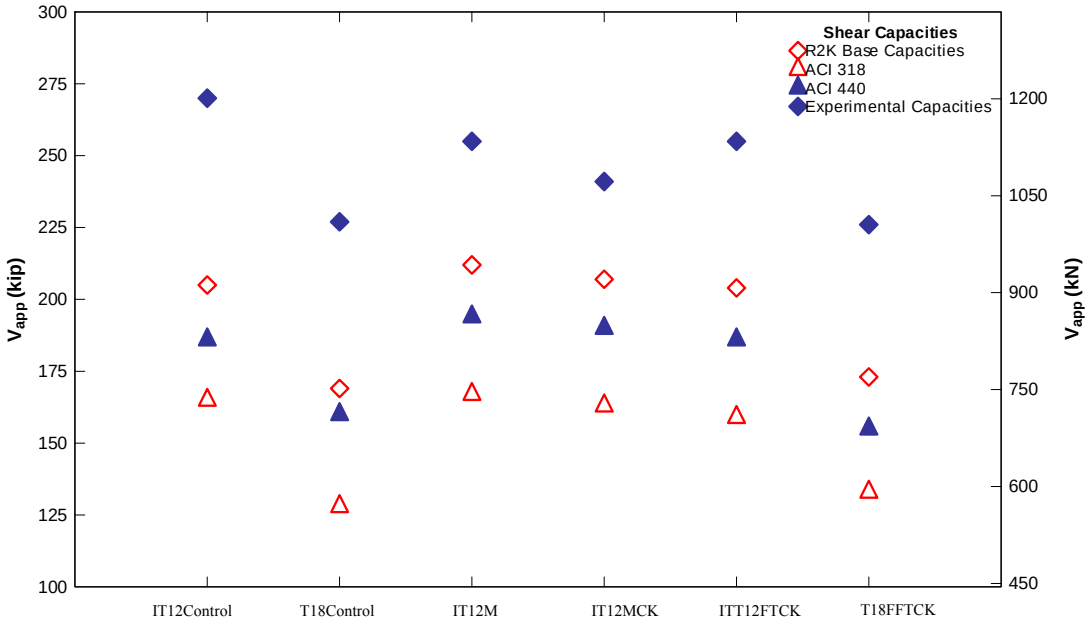

Fig. 6.1 – Shear capacities for all specimens and analysis methods.

Table 6.1: Shear capacity table.

Specimen	V_{EXP} (kN) [kip]	V_{R2k_B} (kN) [kip]	V_{318} (kN) [kip]	$(\psi V_f)_{440}$ (kN) [kip]	V_{440} (kN) [kip]
IT12Control	1201 [270]	912 [205]	707 [165]	120 [27]	827 [186]
T18Control	1010 [227]	752 [169]	569 [128]	142 [32]	712 [160]
IT12M	1134 [255]	943 [212]	743 [167]	120 [27]	832 [194]
IT12MCK	1072 [241]	920 [207]	725 [163]	120 [27]	805 [190]
ITT12FTCK	1134 [255]	907 [204]	707 [159]	120 [27]	734 [186]
T18FFTCK	1005 [226]	774 [174]	592 [133]	142 [32]	716 [155]

Normalizing these values with respect to the concrete and shear reinforcing properties provided, shown in Fig. 6.2, can give some valuable insight. After normalization, the calculated base capacity, V_{318} (kN) [kip], and calculated strengthened specimen capacity, V_{440} (kN) [kip] produce an increase in strength with additional shear reinforcement. Experimental values that fall above this line are conservative with respect to that prediction. Additionally, the shear required to cause flexural failure, V_{flex} (kN) [kip] is shown for both the IT and T specimens assuming a concrete strength of 31 MPa (4500 psi).

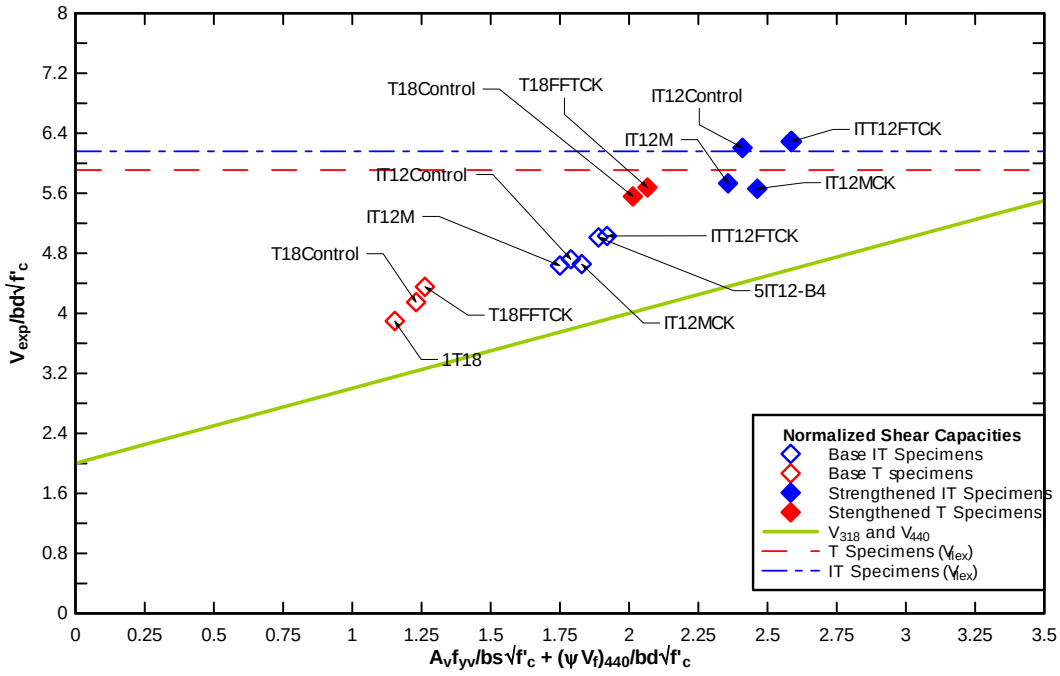

Fig. 6.2 – Normalized shear capacities with ACI prediction.

It can be seen in Fig. 6.2, that while all experimental capacities were conservative with respect to the ACI predictions, the capacities are not well predicted. It should be noted that since the base specimens are conservatively predicted, this conservatism is transferred into the strengthened specimen. The actual calculated CFRP shear contribution may not be conservative when considered independently. Furthermore, as the shear reinforcing quantity increases, the prediction becomes less accurate.

As has been discussed previously, Response-2000 has been shown to predict the unstrengthened base capacity of these specimens well. In order to project the shear response of CFRP strengthened specimens, the shear reinforcing quantities were increased and the resulting R2K strengths were predicted for IT and T specimens. The shear strength

was predicted at the approximate location where the average failure diagonal crack crossed the flexural tension steel and resulted in a M/V ratio of 1524 mm (60 in.) and 1829 mm (72 in.) for the IT and T specimens, respectively. An average concrete compressive concrete strength of 31 Mpa (4500 psi) along with actual flexural and transverse steel properties determined from material testing and reported in Table 4.2 were used in the analysis.

6.4 Estimated CFRP Shear Contribution

The shear contribution of the surface-bonded CFRP was estimated based on the experimental response and the calculated base specimen shear capacity. Two different base capacities were used: ACI-318 and Response-2000. The first prediction used the ACI-318 base strength to estimate the contribution of the CFRP to shear strength, $(V_f)_{ACI\text{-}EXP}$ (kN) [kip], and was determined by subtracting the specimen base capacity determined using ACI-318, V_{318} (kN) [kip], from the measured specimen capacity, V_{EXP} (kN) [kip] as:

$$(V_f)_{ACI-EXP} = V_{EXP} - V_{318} \qquad [6.17]$$

The second prediction used the Response-2000 base capacity to estimate the contribution of the CFRP to shear strength, $(V_f)_{R2k\text{-}EXP}$ (kN) [kip], and was determined by subtracting the estimated base capacity, V_{R2k_B} (kN) [kip], from the strengthened specimen capacity found in testing, V_{EXP} (kN) [kip] as:

$$(V_f)_{R2k-EXP} = V_{EXP} - V_{R2k\_B} \qquad [6.18]$$

Comparison of the estimated CFRP shear contributions, $(V_f)_{ACI\text{-}EXP}$ (kN) [kip] and $(V_f)_{R2k\text{-}EXP}$ (kN) [kip], to the calculated shear contribution, $(\psi V_f)_{440}$ (kN) [kip] is shown in Table 6.2.

Table 6.2: CFRP shear contribution comparison.

Specimen	$(\psi V_f)_{440}$ (kN) [kip]	$(V_f)_{ACI-EXP}$ (kN) [kip]	$\frac{(V_f)_{ACI-EXP}}{\psi V_f}$	$(V_f)_{R2k-EXP}$ (kN) [kip]	$\frac{(V_f)_{R2k-EXP}}{\psi V_f}$
IT12Control	120 [27]	467 [105]	3.89	289 [65]	2.4
T18Control	142 [32]	440 [99]	3.09	258 [58]	1.81
IT12M	120 [27]	391 [88]	3.26	191 [43]	1.6
IT12MCK	120 [27]	347 [78]	2.89	151 [34]	1.26
ITT12FTCK	120 [27]	427 [96]	3.56	227 [51]	1.89
T18FFTCK	142 [32]	414 [93]	2.90	236 [53]	1.65

As seen in this table, the ACI procedure estimates a higher CFRP contribution to shear strength than that determined using a more refined estimate of the base capacity. Using experimental results from Specimens IT12Control and T18Control, the estimated CFRP shear contributions, $(V_f)_{R2k-EXP}$, are 289 kN (65 kips) and 258 (58 kips), respectively, as seen in Table 6.2.

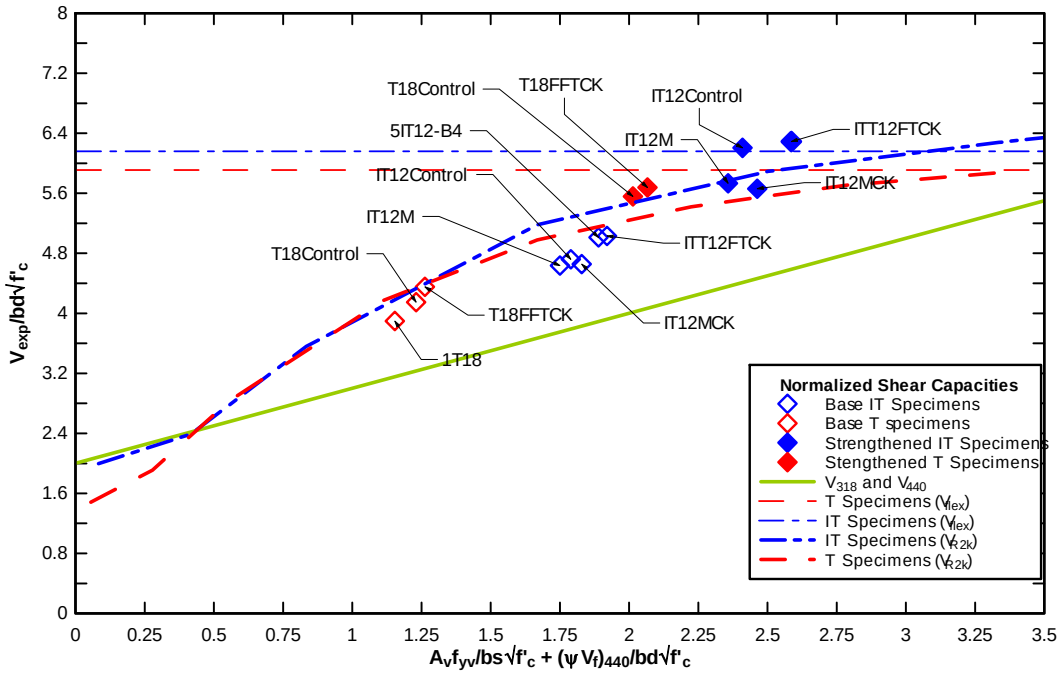

Fig. 6.3 - Normalized shear capacity with $(V_f)_{R2k\text{-}EXP}$.

Response-2000 can be used to predict both the unstrengthened base specimen and strengthened specimen capacity well by adjusting the effective CFRP shear contribution. It would follow that, the CFRP shear contribution used in this case is a better representation of the actual CFRP shear contribution.

6.5 CFRP Effective Stress

Using $(V_f)_{R2k\text{-}EXP}$ (kN) [kips], the experimental CFRP effective stress, $f_{fe\text{-}EXP}$ (Mpa) [ksi] was back calculated for both the IT and T specimens. This is compared to the calculated effective stress, f_{fe} (Mpa) [ksi], using ACI-440 in Table 6.3.

Table 6.3: Comparison of CFRP effective stress.

Specimen	f_{fe} (Mpa) [ksi]	$f_{fe\text{-}EXP}$ (Mpa) [ksi]	$\frac{f_{fe-EXP}}{f_{fe}}$
IT12Control	147 [21]	303 [44]	2.10
T18Control	147 [21]	207 [30]	1.42
IT12M	147 [21]	516 [75]	3.51
IT12MCK	147 [21]	468 [68]	3.23
ITT12FTCK	147 [21]	317 [46]	2.19
T18FFTCK	147 [21]	158 [23]	1.09

As seen in Table 6.3, the CFRP stress calculated from experimental results is approximately twice that calculated using ACI-440 for the IT specimens. For Specimen T18Control, it is approximately 1.5 times greater. However, for the T specimens subjected to freeze-thaw exposure and fatigue, it is approximately that calculated by ACI-440 and indicates a need for additional strength reduction for environmental exposure.

6.6 Average Bond Stress

It was assumed that bond stress increased linearly to the CFRP effective stress over the active bond length, L_e (mm) [in.], so that the average bond stress, τ (Mpa) [ksi], was calculated as:

$$\tau = \frac{f_{fe} t_f}{2L_e} \qquad [6.19]$$

Assuming no change in active bond length for the different exposure conditions, the average bond stress determined by ACI-440 and the experimental bond stress can be calculated. These values are compared in Table 6.4.

Table 6.4: Bond stress comparison

Specimen	t_f (mm) [in.]	L_e (mm) [in]	f_{fe} (MPa) [ksi]	τ (MPa) [ksi]	$f_{fe\text{-}EXP}$ (MPa) [ksi]	τ_{EXP} (MPa) [ksi]
IT12Control	1.16 [0.0458]	48 [1.9]	147 [21]	1.79 [0.26]	303 [44]	3.68 [0.534]
T18Control	1.16 [0.0458]	48 [1.9]	147 [21]	1.79 [0.26]	207 [30]	2.54 [0.368]
IT12M	1.16 [0.0458]	48 [1.9]	147 [21]	1.79 [0.26]	200 [45]	3.80 [0.551]
IT12MCK	1.16 [0.0458]	48 [1.9]	147 [21]	1.79 [0.26]	209 [47]	3.92 [0.568]
ITT12FTCK	1.16 [0.0458]	48 [1.9]	147 [21]	1.79 [0.26]	317 [46]	3.82 [0.55]
T18FFTCK	1.16 [0.0458]	48 [1.9]	147 [21]	1.79 [0.26]	158 [23]	1.98 [0.287]

The values in Table 6.4 show a mostly conservative estimate of bond stress by ACI-440 when compared to experimental results, except in the case of Specimen T18FT and T18FTCK. The specimen with combined fatigue and freeze-thaw resulted bond stress just above that specified by ACI 440 and again indicates a need for some additional conservatism for long-term applications of surface bonded CFRP strips for shear strengthening in climates that experience many freeze-thaw cycles. These average bond stress values were calculated assuming no change in the CFRP active bond length. The active bond length could change based on environmental exposure, but no data from the current tests are available to assess this effect.

7 CONCLUSIONS

Based upon the results of experimental testing and analysis, the following conclusions are presented:

- CFRP application increased the shear capacity of all specimens based on comparison with Response-2000 predictions of the unstrengthened base specimens and previous testing of similar unstrengthened specimens.
- Overall member stiffness (applied shear versus midspan displacement) was not affected by the application of CFRP shear reinforcing.
- Shear panel stiffnesses (applied shear versus average vertical strain), measured using displacement sensors oriented along the panel diagonals, increased due to the application of CFRP shear reinforcing. This increased stiffness indicated reduced diagonal crack widths, which were observed during testing.
- The IT specimens did not exhibit strength reductions due to moisture exposure, instead the presence of continuous water exposure for the relatively young concrete caused higher concrete tensile properties resulting in increased bond strength.
- The presence of moisture at the CFRP-concrete bond interface during freeze-thaw cycling was detrimental to bond strength while freeze-thaw cycling with no moisture at the bond interface did not affect the strength of the specimens.
- CFRP strengthened T specimens subjected to freeze-thaw exposure demonstrated a change in shear panel stiffness (applied shear versus average vertical strain) from pre-exposure response to post-exposure response. This decrease in stiffness was

attributed to increases in debonded areas of the CFRP strips incurred during freeze-thaw exposure. CFRP strengthened T specimens subjected to the combined action of freeze-thaw and fatigue had more pronounced effect of debonding.

- The orientations of specimens during repair and during exposure are important considerations for environmental durability. The CFRP strip terminations should be focused on during installation to insure well and perhaps extra saturation even past the CFRP material to limit moisture infiltration along this edge.
- Even though epoxy injection does not increase the capacity of the beam, it plays an important role of keeping moisture from freely moving through the cracks in the beam. After failure, moisture was clearly seen to have been arrested at the injected cracks for the moisture specimens.
- Previously, CFRP strengthened T specimens subjected to freeze-thaw exposure have exhibited less shear capacity than the unexposed CFRP strengthened T specimen. But if the beam is well protected against moisture infiltration from the strip termination, the beam will be less susceptible to freeze-thaw bond deterioration.
- The combined actions of fatigue and freeze-thaw did not exhibit strength reductions as the CFRP terminated at edges were well protected saturant that prevented moisture ingress. The stress levels induced by fatigue loading were sufficient to increase the debonded CFRP strip regions, showing a gradual loss of stiffness. However, the CFRP stresses were not sufficient to disturb the CFRP bonding along the top near the terminations and thus did not reduce overall member strength.

- ACI-318 conservatively predict the unstrengthened base shear capacity of the specimens compared to the capacities predicted by Response-2000 and shown in previous tests at Oregon State University.
- Response-2000 appeared to predict the capacity of the unstrengthened base specimens well. This allowed for a more refined estimate of the CFRP contribution.
- When ACI-318 was considered to predict the base capacity of the specimens, the CFRP shear contribution calculated from ACI-440 was conservative when compared to the experimental shear contribution for all specimens. This conservatism may be misleading as it is partially due to the conservatism in the prediction of the unstrengthened base specimen.
- When Response-2000 was considered to predict the base capacity of the specimens, the CFRP shear contribution calculated from ACI-440 appeared to be conservative when compared to the experimental shear contribution for all specimens although less so for the specimen subjected to combined freeze-thaw and fatigue. This indicates that some additional conservatism may be warranted in the current design provisions.

8 RECOMMENDATIONS

8.1 CFRP Shear Strengthening

The previous conclusions based on experimental results and comparative analysis, lead to the following recommendations regarding CFRP strengthening:

- Development of a more accurate prediction of surface-bonded CFRP shear contribution is warranted with consideration given to environmental exposure.
- The ACI-440 calculated CFRP shear contribution should only be superimposed with unstrengthened base capacities calculated with ACI-318, to which it is calibrated. Superimposition with refined unstrengthened base capacity predictions may lead to unconservative results.
- CFRP strengthened bridges in regions of high freeze-thaw exposure should be routinely monitored for increased debonding of the CFRP as this may indicate decreased capacity.
- Prevention of moisture ingress is key to long-term freeze-thaw durability. Exterior girders would be more susceptible to moisture exposure. Where cracks or debonding are identified during routine inspections, these should be remediated to prevent moisture infiltration.

8.2 Future Testing

The results of this testing protocol warrant further testing and examination of the durability of RCDG bridge member strengthened for shear with surface-bonded CFRP under freeze-thaw exposure. The following recommendations are made for future testing:

- Specimens with even lower transverse steel shear contributions should be investigated to enable shear failure with increased CFRP shear contribution. Specimens should still conform to minimum transverse steel requirements.
- Specimens should be precracked as this is representative of field applications.
- Specimens should be reloaded after strengthening, to produce recracking, prior to freeze-thaw exposure.
- Specimens should be strengthened and be subjected to freeze-thaw exposure in the T orientation as they would be in the field.
- Additional data are needed for combined environmental exposure and fatigue loading.

9 REFERENCES

American Concrete Institute, 2002, "440.2R-02: Design and construction of externally bonded FRP systems," *ACI Manual of Concrete Practice*, Farmington Hills, Michigan.

American Concrete Institute, 2005, "318-05: Building code requirements for structural concrete and commentary," *ACI Manual of Concrete Practice*, Farmington Hills, Michigan.

ASTM A 370-97a, American Society of Testing and Materials, "Standard Test Methods and Definitions for Mechanical Testing of Steel Products," ASTM, West Conshohocken, PA, 1997.

ASTM C 666-97, American Society of Testing and Materials, "Standard Test Method for Resistance of Concrete to Rapid Freezing and Thawing," ASTM, West Conshohocken, PA, 1997.

ASTM D 3039/D 3039M-00, American Society of Testing and Materials, "Standard Test Method for Tensile Properties of Polymer Matrix Composite Materials," ASTM, West Conshohocken, PA, 2001.

ASTM D 4541-02, American Society of Testing and Materials, "Standard Test Method for Pull-Off Strength of Coatings Using Portable Adhesion Testers," ASTM, West Conshohocken, PA, 2002.

ASTM E 8-00, American Society of Testing and Materials, "Standard Test Methods for Tension Testing of Metallic Materials," ASTM, West Conshohocken, PA, 2000.

Bentz, D. P., 2000, "A computer model to predict the surface temperature and time-of-wetness of concrete pavements and bridge decks," NISTIR 6551, U.S. Department of Commerce.

Bentz, E.C., 2001, "Membrane-2000, Response-2000, Triax-2000, Shell-2000 User Manual," University of Toronto, <http://www.ecf.utoronto.ca/~bentz/manual.shtml>.

Bisby, L. A., and Green, M. F., 2002, "Resistance to freezing and thawing of fiber-reinforced polymer-concrete bond," *ACI Structural Journal,* V 99, No. 2, pp. 215-223.

Chajes, M. J., Thomson, T. A., and Farschman, C. A., 1995, "Durability of concrete beams externally reinforced with composite fabrics," *Construction and Building Materials,* V 9, No. 3, pp. 141-148.

Dawson, M.R., 2008, *Scale Effects on Reinforced Concrete Beams Strengthened for Shear with Discrete Externally Bonded Carbon Fiber-Reinforced Polymer U-Wraps*, Master's thesis, Oregon State University.

Dutta, P. K., 1992, "Tensile strength of unidirectional fiber composites at low temperatures," *6th Japan-U.S. Conference on Composite Materials, Proceedings,* Orlando, pp. 782-792.

Dutta, P. K., 1995, "Durability issues of FRP composites in offshore structures," *5th International Offshore and Polar Engineering Conference, Proceeedings,* V. 4, Hague, Netherlands, pp. 271-277.

Grace, N. F., and Singh, S. B., 2005, "Durability evaluation of carbon fiber-reinforced polymer strengthened concrete beams: experimental study and design," *ACI Structural Journal,* V 102, No. 1, pp. 40-53.

Green, M. F., Bisby, L. A., Beaudoin, Y., and Labossiere, P., 1998, "Effect of freeze-thaw action on the bond of FRP sheets to concrete," *Proceedings of the First International Conference on Durability of Composites for Construction,* Sherbrooke, Quebec, pp. 179-190.

Green, M. F., Bisby, L. A., Beaudoin, Y., and Labossiere, P., 2000, "Effect of freeze-thaw cycles on the bond durability between FRP plate reinforcement and concrete," *Canadian Journal of Civil Engineering,* V 27, pp. 949-959.

Green, M. F., Dent, A. J. S., and Bisby, L. A., 2003, "Effect of freeze-thaw cycling on the behaviour of reinforced concrete beams strengthened in flexure with fibre reinforced polymer sheets," *Canadian Journal of Civil Engineering,* V 30, pp. 1081-1088.

Higgins, C., Miller, T.H., Rosowsky, D.V., Yim, S.C., Potisuk, T., Daniels, T.K., Nicholas, B.S., Robelo, M.J., Lee, A-Y, and R.W. Forrest, 2004, "Assessment Methodology for Diagonally Cracked Reinforced Concrete Deck Girders," Report No. FHWA-OR-RD-05-04, U.S. Department of Transportation Federal Highway Administration.

Higgins, C., Williams, G., and Elkins, L., 2006, "Capabilities of Diagonally-Cracked Girders Repaired with CFRP," *Report* No. FHWA-OR-RD-06-16, U.S. Department of Transportation Federal Highway Administration.

Incropera, F., and DeWitt, P., *Introduction to Heat Transfer*, John Wiley & Sons, New York, 2002.

Holman, J.P., *Heat Transfer*, McGraw-Hill Inc., New York, 1997.

Lord, H. W., and Dutta, P. K., 1988, "On the design of polymeric composite structures for cold regions applications," *Journal of Reinforced Plastics and Composites,* V 7, pp. 435-458.

MacGregor, J. G. and Wight, J. K., *Reinforced Concrete Mechanics and Design*, Pearson Prentice Hall, New Jersey, 2005.

Motavalli, M., Terrasi, G. P., and Meier, U., 1993, "On the behavior of hybrid aluminum/CFRP box beams at low temperatures," Swiss Federal Laboratories for Materials Testing and Research (EMPA), Switzerland.

Mukhopadhyaya, P., Swamy, R. N., and Lynsdale, C. J., 1998, "Influence of aggressive exposure conditions on the behaviour of adhesive bonded concrete-GFRP joints," *Construction and Building Materials,* V 12, pp. 427-446.

Schlangen, E, 2000, "Online help/manual module HEAT of FEMMASSE," The Netherlands.

Soudki, K. A., and Green, M. F., 1997, "Freeze-thaw response of CFRP wrapped concrete," *Concrete International,* V 19, No. 8, pp. 64-67.

Watson Bowman Acme Corporation, "Specification: Wabo® MBrace Composite Strengthening System with Carbon Fiber Reinforcement," Amherst, NY, March 2002.

Watson Bowman Acme Corporation, "Wabo® MBrace CF130," Amherst, NY, February 2003.

10 NOTATION

A_{fv}	=	area of FRP shear reinforcement with spacing s_f, (mm^2) [$in.^2$]
A_s	=	area of flexural-tension steel reinforcement (mm^2) [$in.^2$]
A_v	=	area of transverse steel reinforcement within spacing, s (mm^2) [$in.^2$]
b_w	=	beam web width (mm) [in.]
c	=	specific heat (J/kg·°C) [Btu/lb·°F]
C_E	=	environmental reduction factor
d	=	effective depth, distance from extreme compression fiber to centroid of flexural-tension steel reinforcement (mm) [in.]
d_f	=	effective depth of FRP shear reinforcement (mm) [in.]
E_f	=	tensile modulus of elasticity of FRP (GPa) [ksi]
E_{fu}	=	ultimate tensile modulus of elasticity of FRP (GPa) [ksi]
E_{fu}*	=	tensile modulus of elasticity of FRP based on nominal fabric thickness (GPa)[ksi]
$f_{pull\text{-}off}$	=	direct tension pull-off strength of FRP bonded to concrete (MPa) [psi]
f_c'	=	specified compressive strength of concrete (MPa) [psi]
f_{fe}	=	effective FRP tensile strength (MPa) [ksi]
$f_{fe\text{-}EXP}$	=	estimated CFRP effective stress calculated from experimental results (MPa) [ksi]
f_{fu}	=	design ultimate FRP tensile strength (MPa) [ksi]
f_{fu}^*	=	design ultimate FRP tensile strength provided by manufacturer (MPa) [ksi]
f_t	=	concrete split cylinder tensile strength (MPa) [ksi]
f_{ult}	=	ultimate tensile strength of reinforcing steel (MPa) [ksi]
f_y	=	yield strength of steel reinforcement (MPa) [ksi]

f_{yt} = yield strength of transverse steel reinforcement (MPa) [ksi]

h = convection heat transfer coefficient ($W/m^2 \cdot °C$) [$Btu/hr \cdot ft^2 \cdot °F$]

k = thermal conductivity ($W/m \cdot °C$) [$Btu/hr \cdot ft \cdot °F$]

k_1 = modification factor applied to κ_v for concrete strength

k_2 = modification factor applied to κ_v for FRP wrapping scheme

L = overall length (mm) [in.]

L_e = effective bond length of FRP laminate (mm) [in.]

n = number of plies of FRP reinforcement

s = spacing of transverse steel reinforcement

s_f = spacing of FRP shear reinforcement (mm) [in.]

t_f = nominal thickness of one ply of FRP reinforcement (mm) [in.]

t_f* = nominal FRP fabric thickness (mm) [in.]

V = shear force (kN) [kips]

V_{318} = unstrengthened base specimen shear capacity calculated using ACI-318(kN) [kips]

V_{440} = CFRP strengthened specimen shear capacity calculated using ACI-318 and ACI-440 (kN) [kips]

V_{app} = applied shear force (kN) [kips]

V_c = nominal shear strength provided by concrete with steel flexural reinforcement (N) [lbs]

V_{DL} = self weight of the specimen acting at the failure crack (kN) [kips]

V_{EXP} = sum of applied shear and specimen dead load (kN) [kips]

$V_{ACI-EXP}$= estimated CFRP shear contribution using ACI-318 base capacity (kN) [kips]

$V_{R2k\text{-}EXP}$ = estimated CFRP shear contribution using R2k base capacity (kN) [kips]

V_{flex} = shear required to cause flexural failure (kN) [kips

V_f = nominal shear strength provided by FRP shear reinforcement (N) [lbs]

V_n = nominal shear strength (kN) [kips]

V_{R2k_B} = unstrengthened base specimen shear capacity predicted by Response-2000 (kN) [kips]

V_s = nominal shear strength provided by transverse steel reinforcement (N) [lbs]

w_f = width of FRP reinforcing plies (mm) [in.]

x_{max} = maximum out-of-plane deformation (mm) [in.]

α = inclination angle of stirrups (degrees)

ε_{fe} = effective strain level in FRP reinforcement; strain level at section failure (mm/mm) [in./in.]

ε_{fu}^{*} = design rupture strain of FRP reinforcement provided by manufacturer (mm/mm) [in./in.]

ε_{fu} = design rupture strain of FRP reinforcement (mm/mm) [in./in.]

ρ = density (kg/m^3) [lb/ft^3]

τ = average bond stress (Mpa) [ksi]

τ_{EXP} = estimated average bond stress calculated from experimental results (Mpa) [ksi]

ϕ = strength reduction factor

κ_v = bond-dependent coefficient for shear

ψ_f = additional FRP strength reduction factor

Appendix A

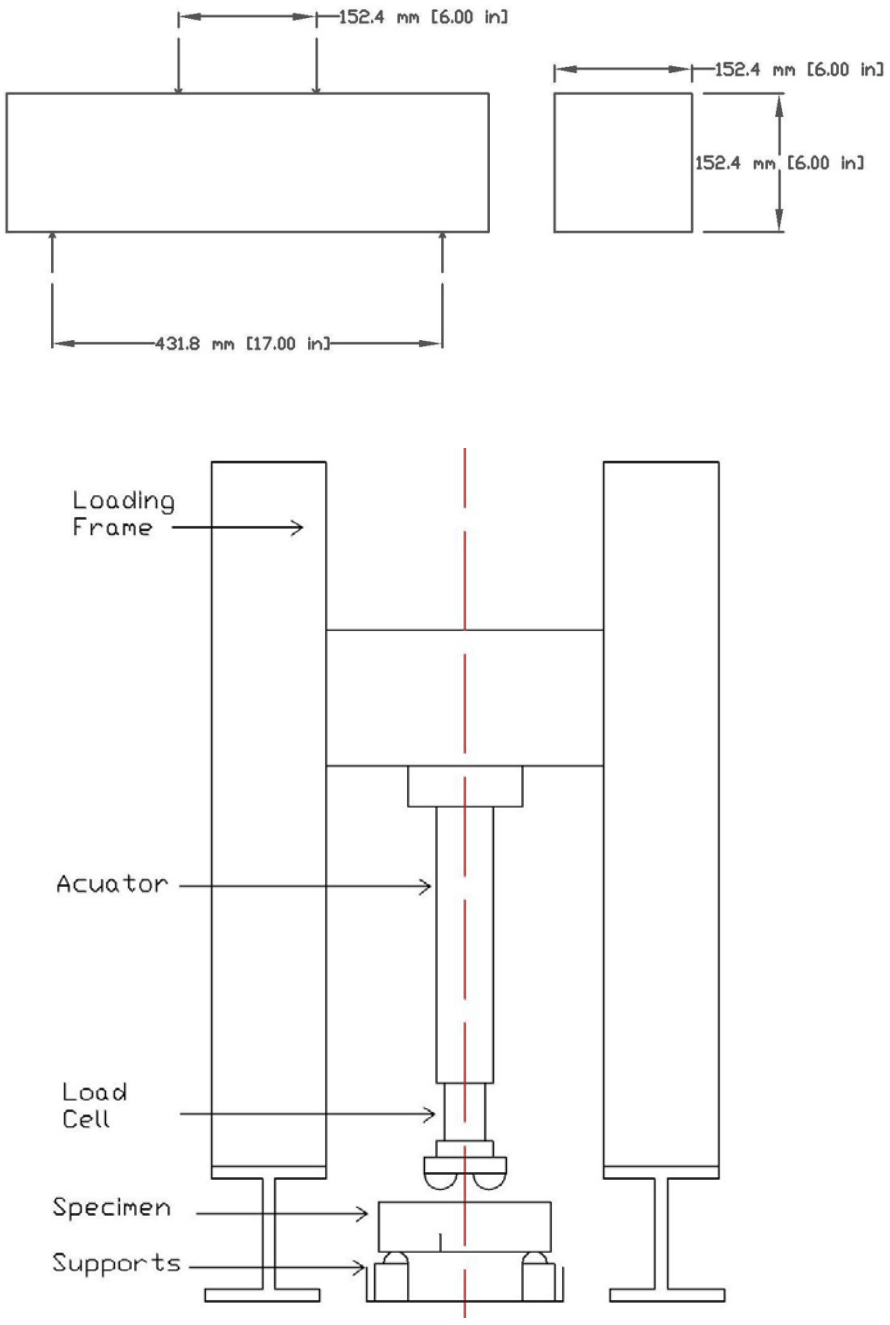

Fig A-1 Loading Setup and typical specimen

Table A-1 Bond Specimens

CFRP System	MBrace	Sika	Fyfe	Edge
Control	3	3	3	3
Moisture	3	3	3	3
Freeze-Thaw	3	3	3	3

A-1: CFRP Application Fyfe System

Fyfe CFRP system was installed according to *Fyfe Co. LLC Quality Control Manual.* Surface preparation process is same for all kind of CFRP systems. After surface was prepared, Tyfo S Epoxy was made by using premixed 100 parts of component A and 42 parts of component B by volume (100 parts of component A to 34.5 parts of component B by weight). The two components were then mixed thoroughly for five minutes with a low speed mixer until uniformly blended. A base coat of Tyfo S epoxy was then applied to the surface, first making sure the surface was clean and free of debries. Pre-cut lengths of Tyfo SCH fabric was then saturated in manually built saturation bath tub, made out with sheet of plywood and two-by-fours. A piece of PVC pipe was used to spool the saturated fabric for transportation over the prisms.

A-2 : CFRP Application Edge System

After preparing surface as described previously, a coat of primer is applied prior to the application of epoxy saturating resin. Using a roller, a coat of mixed resin was applied to a suitable worktable, which has been protected with plastic sheeting. A pre-cut fabric was laid onto resin coat and press down with a soft plastic spreader. More resin was applied to

the fabric and spread evenly until fabric was fully covered and saturated thoroughly with resin. Then it was allowed to sit for 1 minute, applying more resin if needed. A PVC plastic putty knife was used to Squeegee off excess resin if necessary and roll fabric onto.

A-3 : CFRP Application Sika System

Each component of Sikadur Hex 300 was pre-mixed. As batching was not allowed, entire unit was mixed, contents of part 'B' to part 'A' until uniformly blended. Rest of the procedure is just similar to Edge installation system.